UNIVERSIDADE ESTADUAL PAULISTA
"JÚLIO DE MESQUITA FILHO"
Campus de Ilha Solteira

Pedro Christian Ayala Castillo

DETECÇÃO DE DANOS EM ESTRUTURAS GUIADAS USANDO ONDAS DE ALTA FREQUÊNCIA

Ilha Solteira

2015

UNIVERSIDADE ESTADUAL PAULISTA
"JÚLIO DE MESQUITA FILHO"
Campus de Ilha Solteira

Pedro Christian Ayala Castillo

DETECÇÃO DE DANOS EM ESTRUTURAS GUIADAS USANDO ONDAS DE ALTA FREQUÊNCIA

Dissertação apresentada à Faculdade de Engenharia – UNESP – Campus de Ilha Solteira, para obtenção do título de Mestre em Engenharia Mecânica.

Área de Conhecimento: Mecânica dos Sólidos

Prof. Dr. Vicente Lopes Junior

Orientador

Prof. Dr. Michael John Brennan

Co-Orientador

Ilha Solteira

2015

A973d

Ayala Castillo, Pedro Christian.

Detecção de danos em estruturas guiadas usando ondas de alta frequência / Pedro Christian Ayala Castillo. -- Ilha Solteira: [s.n.], 2015

83 f. : il.

Dissertação (mestrado) - Universidade Estadual Paulista. Faculdade de Engenharia de Ilha Solteira. Área de conhecimento: Mecânica dos Sólidos , 2015

Orientador: Vicente Lopes Júnior

Co-orientador: Michael John Brennan

Inclui bibliografia

1. Propagação de ondas. 2. Ondas de alta frequência . 3. Detecção de danos. 4. Descontinuidade em estruturas. 5. Onda longitudinal e de flexão . 6. Monitoramento de integridade estrutural.

unesp UNIVERSIDADE ESTADUAL PAULISTA
CAMPUS DE ILHA SOLTEIRA
FACULDADE DE ENGENHARIA DE ILHA SOLTEIRA

CERTIFICADO DE APROVAÇÃO

TÍTULO: DETECTION OF DAMAGE IN STRUCTURAL WAVEGUIDES USING HIGH FREQUENCY WAVES

AUTOR: PEDRO CHRISTIAN AYALA CASTILLO
ORIENTADOR: Prof. Dr. VICENTE LOPES JUNIOR
CO-ORIENTADOR: Prof. Dr. MICHAEL JOHN BRENNAN

Aprovado como parte das exigências para obtenção do Título de Mestre em Engenharia Mecânica , Área: MECANICA DOS SÓLIDOS, pela Comissão Examinadora:

Prof. Dr. MICHAEL JOHN BRENNAN
Departamento de Engenharia Mecânica / Faculdade de Engenharia de Ilha Solteira

Prof. Dr. FABRICIO CÉSAR LOBATO DE ALMEIDA
Departamento de Engenharia Mecânica / Faculdade de Engenharia de Ilha Solteira

Prof. Dr. JOSÉ ROBERTO DE FRANÇA ARRUDA
Departamento de Mecanica Computacional / Universidade Estadual de Campinas

Data da realização: 28 de abril de 2015.

Dedication

I dedicate this dissertation to my loving and admirable wife, Liesel.

ACKNOWLEDGEMENTS

I would like to take this opportunity to express my sincere gratitude to my excellent supervisor, Professor Mike Brennan for his kind-hearted, rigorous and patient supervision, his comments and unfaltering guidance has made this work possible and enjoyable. I would like also to thank Professor Vicente Lopes, he believe in me and who first introduce me to the GMSINT group, always giving me advices and unconditional support during my studies of master.

I would like to thank Professor Bin Tang; I found his additional input from another point of view very helpful in my work and his advices that are helping me to achieve my goals. I would like to thank Laura Brennan for her help and friendship, her lessons and our conversations are helping me to be better every day.

Special thanks to my lovely wife Liesel and my family who have always stood by me in whatever I have ever done.

I would like to thank Capes (Coordenação de Aperfeiçoamento de Pessoal de Nível Superior) for the financial support.

“The scientist does not study nature because it is useful; he studies it because he delights in it, and he delights in it because it is beautiful. If nature were not beautiful, it would not be worth knowing, and if nature were not worth knowing, life would not be worth living.”

- Henri Poincaré

RESUMO

Pesquisas em propagação de ondas para aplicação de monitoramento de integridade estrutural (SHM) tem tido um incremento considerável recentemente. Este procedimento permite detectar danos nas fases iniciais. Esta dissertação descreve um estudo teórico de propagação de ondas para o propósito de detecção e quantificação de dano em uma viga. De particular interesse é a maneira que as ondas interagem com o dano, considerado simétrico com respeito ao eixo neutro. Uma análise de uma estrutura unidimensional de ondas guiadas incorporando o atuador e sensores piezelétricos em configuração *pitch-catch* e *pulse eco* é apresentada. O modelo é desenvolvido no domínio da frequência e posteriormente transformado no domínio do tempo através da transformada de Fourier inversa. Isto permite que o efeito do dano entre o atuador e o sensor seja estudado no domínio do tempo e da frequência. Os comprimentos do atuador e do sensor e a profundidade do dano são estudados em uma viga de alumínio delgada. Mostra-se que uma abordagem no domínio do tempo é preferível em relação a abordagem no domínio da frequência para detecção e quantificação de danos na estrutura. Os resultados mostraram que ondas longitudinais são mais sensíveis a variação da espessura para um sistema simétrico e é melhor medir ondas refletidas que as transmitidas. Além disto, verificou-se que devido à natureza dispersiva das ondas de flexão é possível que em algumas situações a amplitude da onda refletida seja diminuída em vez de aumentar quando a espessura da viga é reduzida.

Palavras-chave: Monitoramento de integridade estrutural. Ondas de alta frequência. Interferência de onda.

ABSTRACT

Wave propagation research for Structural Health Monitoring (SHM) has been increasing recently. It allows the detection of damage at its early stages of development. This dissertation describes a theoretical study of wave propagation for the purpose of detection and quantification of damage in a beam structure. Of particular interest is the way in which waves interact with damage that is symmetrical with respect to the neutral axis. An analysis of a one-dimensional structural waveguide incorporating a piezoelectric actuator and sensors in a pitch-catch and pulse-echo configuration is presented. The model is developed in the frequency domain, which is then transformed into the time domain using the inverse Fourier transform. This enables the effect of damage on wave propagation between the actuator and the sensor to be investigated in both the time and the frequency domains. The size of the actuator and the sensor, and the size of damage are investigated for a thin aluminum beam. It is shown that the time-domain approach is preferable to a frequency domain approach for damage detection in this kind of structure. It is found that longitudinal waves are more sensitive to a change in thickness for a symmetrical system and it is better to measure reflected rather than transmitted waves. Further, it is found that due to the dispersive nature of bending waves, it is possible in some situations for the reflected wave amplitude to decrease rather than increase as the beam thickness is reduced.

Keywords: Structural health monitoring. High frequency waves. Wave interference.

LIST OF SYMBOLS

Symbol	Name	Units
A_l	Longitudinal Amplitude going to the left	$[-]$
A_r	Longitudinal Amplitude going to the right	$[-]$
A_1	Evanescent Amplitude going to the left	$[-]$
A_2	Evanescent Amplitude going to the right	$[-]$
A_3	Flexural amplitude going to the left	$[-]$
A_4	Flexural amplitude going to the right	$[-]$
A_{R1}	Incident propagating flexural amplitude going to the left	$[-]$
A_{R3}	Incident evanescent amplitude going to the left	$[-]$
A_{Rl}	Incident propagating longitudinal amplitude going to the left	$[-]$
A_{L2}	Incident evanescent amplitude going to the left	$[-]$
A_{L4}	Incident propagating flexural amplitude going to the left	$[-]$
A_{Lr}	Incident propagating longitudinal amplitude going to the right	$[-]$
A_{L1}	Reflected propagating flexural amplitude going to the left	$[-]$
A_{L3}	Reflected evanescent amplitude going to the left	$[-]$
A_{L3}	Reflected propagating longitudinal amplitude going to the left	$[-]$
A_{R2}	Transmitted propagating flexural amplitude going to the right	$[-]$
A_{R4}	Transmitted evanescent amplitude going to the right	$[-]$
A_{Rr}	Transmitted propagating longitudinal amplitude going to the right	$[-]$
b	Width of the beam	$[\mathrm{m}]$
b_p	Width of the piezoelectric elements	$[\mathrm{m}]$
c	Capacitance of the piezoelectric elements	$[\mathrm{C^2/Nm}]$
c_F	Phase velocity of flexural wave	$[\mathrm{m/s}]$
c_{gF}	Group velocity of flexural wave	$[\mathrm{m/s}]$
c_l	Phase velocity of longitudinal wave	$[\mathrm{m/s}]$
$\hat{d}$	Ratio of PZT thickness to beam Thickness	$[-]$
d_{31}	Piezoelectric constant	$[\mathrm{C/N}]$

E	Young's Modulus of beam	$\left[\mathrm{N/m^2}\right]$
E_p	Young's Modulus of piezoelectric	$\left[\mathrm{N/m^2}\right]$
f	Frequency	$[\mathrm{Hz}]$
F	Axial Force	$[\mathrm{N}]$
j	$\sqrt{(-1)}$	
h	Depth of the beam	$[\mathrm{m}]$
h_p	Depth of the piezoelectric	$[\mathrm{m}]$
I	Second moment of area	$\left[\mathrm{m^4}\right]$
k_l	Longitudinal wavenumber	$\left[\mathrm{m^{-1}}\right]$
k_f	Flexural wavenumber	$\left[\mathrm{m^{-1}}\right]$
l	Length of the beam	$[\mathrm{m}]$
l_a	Length of the actuator	$[\mathrm{m}]$
l_p	Length of the piezoelectric element	$[\mathrm{m}]$
l_s	Length of the sensor	$[\mathrm{m}]$
l_D	Length of Damage	$[\mathrm{m}]$
M	Bending Moment	$[\mathrm{Nm}]$
N	Number of samples in each signal	$[-]$
S	Cross sectional-Area of the beam	$[\mathrm{m}]$
t	Time	$[\mathrm{s}]$
u	Longitudinal displacement	$[\mathrm{m}]$
w	Lateral displacement	$[\mathrm{m}]$
V_{out}	Output voltage	$[\mathrm{V}]$
V_{in}	Input voltage	$[\mathrm{V}]$
y_i	Signal amplitude of the structure analysed	$[-]$
$y_{b(i)}$	Signal amplitude of the baseline	$[-]$
θ	Slope of the beam	$[\mathrm{rad}]$
λ	Wavelength	$[\mathrm{m}]$
ρ	Density of the beam	$\left[\mathrm{kg/m^3}\right]$

ψ	Ratio of stiffness	$[-]$
ω_c	Carrier frequency	$[\text{m/s}]$
ω	Angular frequency	$[\text{rad/s}]$
$\mathbf{a}$	Vector of wave amplitude	
$\mathbf{h}$, $\mathbf{v}$	State vector	
$\mathbf{H}$, $\mathbf{V}$	Transformation matrix	
$\mathbf{T}_D$	Spatial transformation Matrix of the Discontinuity	
Subscripts		
B	Denotes beam	
D, d	Denotes damage	
In	Denotes input	
Out	Denotes output	
Superscripts		
R, L	Denotes going to the Right or Left–hand junctions	
T	Denotes transpose	

CONTENT

1 INTRODUCTION

1.1 Background

Engineering structures such us aircraft, bridges, power generation systems, rotary machinery, off shore oil platforms, buildings and defence systems need techniques for damage detection to ensure structural integrity and safety (FARRAR; WORDEN, 2013).

In recent years, the use of wave propagation for structural Health Monitoring (SHM) has been of increasing interest and is the subject of this dissertation. The aim of SHM is to detect damage in its early stages of development. High frequency waves are generated that interact with the damage and the way in which the wave changes, as it interacts with the damage, is used to detect the damage (OSTACHOWICZ et al., 2012).

Many structures have components made of beams and bars, which have a uniform cross-section with homogeneous physical and geometric properties. It is the detection quantification of damage in such structures that is investigated in this dissertation.

1.2 Structural Health Monitoring

Recently the field of SHM has emerged to determine the current state of the health of a structure, identifying four characteristics related to the fitness of an engineered component (or system) as it operates (ADAMS, 2007).

- The operational and environmental loads that act on the component (or system),
- The mechanical damage that is caused by that loading,
- The growth of damage as the component (or system) operates, and
- The future performance of the component (or system) as damage accumulates.

The identification of damage is cited by Doebling, Farrar and Prime (1998), with four levels as follows:

- Level 1 Detect damage in the structure;
- Level 2 Detect and locate damage in the structure;

- Level 3 Detect, locate and quantify damage in the structure;
- Level 4 Detect, locate, quantify damage and predict the remaining service life of the structure.

Inman (2001) adds three levels more, incorporating smart materials:

- Level 5 use of level 4 with smart materials for auto-diagnostic of damage in structures;
- Level 6 use of level 4 with smart materials and control for obtaining a system of auto-repaired of damage in structures;
- Level 7 use of level 1 with active control and smart materials for obtaining simultaneous control and monitoring.

The effects of damage on a structure can be classified as linear or nonlinear. The work described in this dissertation focuses on a linear system. In this case, the initially linear-elastic structure remains linear-elastic after damage, so the structure can be modelled using a linear equation of motion. Nonlinear damage is defined as the case when the initially linear-elastic structure behaves in a nonlinear manner after the damage has occurred (DOEBLING et al., 1996).

1.2.1 Wave propagation in structural Health Monitoring

This method relies on the fact that waves packets are generated in the structure and these waves propagate until they encounter any discontinuity. They can be edges or stiffening elements, but they can also be damage sites. After interacting with discontinuities, waves are reflected and transmitted from them. This behaviour provides the information about the location, size and type of damage; this information is extracted from measured signals by appropriate algorithms (OSTACHOWICZ et al., 2012).

Wave methods belong to the group of local methods because they monitor a determined area without the need for disassembly. They are applied to critical structures, where the high cost of SHM system is acceptable (STEPINSKI; UHL; STASZEWSKI, 2013).

1.3 Literature Review

Modelling allows a real system to be represented theoretically, allowing loads and sensor types to be investigated together with the proper handling of input and output data. These data can be used to study the detection, location, quantification and prediction of structural damage.

Nowadays, theoretical studies are conducted by the way of numerical and analytical methods. Mathematical models have been developed to allow the comprehension of the physical behaviour of wave propagation applied to industrial problems.

Work by Mace (1984) discussed the vibrational behaviour of beam systems in terms of wave propagation. He described the relationships between the wave amplitudes at various positions on the beam, and emphasized the importance of nearfield waves close to discontinuities.

Models developed by Crawley and Anderson (1990), and Wang and Rogers (1991) on piezoelectric (PZT) actuators, were used by Brennan (1994) in the active control of wave motion in beams. These models are used in this dissertation to couple PZT actuators to the beam. The models are also modified to characterize damage in an Euler-Bernoulli Beam.

Rousseau, Mace and Waters (2003) investigated a method for crack identification based on wave propagation in the audible frequency range. This damage was modelled with a rotational spring, to study its effect on a flexural wave both analytically and experimentally. The identification of damage was obtained using the reflection coefficients of propagating waves and experimentally by filtering of the output of an array of sensors. The location of the crack was estimated by measurements made at different positions on the beam.

Lee and Staszewski (2003) developed a model with the wave propagation approach using Lamb waves in metallic structures. They analysed applications of damage detection. The study involves wave propagation in a piezoceramic actuator/sensor diffusion bond model in which one of the piezoceramics generates the thickness mode vibration. The simulated results are validated experimentally. The results show the potential of the method for wave propagation analysis in damage detection applications.

Raghavan and Ceznik (2004) explored the modelling of transient plane and circular-crested Lamb-wave generation and sensing for structural health monitoring, using a surfacebonded piezo element in isotropic plates based on the 3-D linear equations. Optimization of the geometry of the piezoelectric elements and materials was done based on equations of the output voltage response. Numerical and experimental results validated of the models.

Cawley and Allenyne (2004) carried out damage detection in examples such as in a pipe, rail and plate testing. Many possible waves modes, most of which were dispersive were present and this can cause problems. It was shown that an array of transducers acting as a point source provides a basis from which these problems can be overcome.

Shone (2006) explored the use of wave scattering for damage detection in beams. Specifically he used scattering coefficients as a feature for diagnosis of transverse slots cut into the beam i.e., estimating existence, depth and location. Analytical, numerical and experimental methods were analysed, achieving a good degree of accuracy.

In the same year (2006), Lee developed a systematic formulation of the wave approach based on scattering waves for the analysis of one-dimensional structures. He studied the behaviour of uniform structures such as curved beams, with constant curvature. Applications of the wave approach are illustrated for several elementary structures. It is shown that the wave approach can be used as an efficient and well-conditioned computational method.

Numerical simulations with the Finite Element Method (FEM) and experimental tests were carried out by Giurgiutiu (2008) using pairs of Piezoelectric Wafer Active Sensors (PWAS) in a one-dimensional guided structure. Axial and flexural waves in the pulse-echo configuration were studied.

Michaels, Ruzzeneb and Michaels (2009) used frequency wavenumber domain methods for the analysis of incident and scattered guided wave fields. This demonstrated a method to enhance acoustic wavefield images for determining the scattering pattern from a through hole with a notch added to simulate a fastener hole in an aluminium plate specimen.

Wang et al. (2010) carried out an experimental investigation of reflection in guided wave-based inspection from a defect in a pipeline. They found that the reflection of guided waves at a defect is the combined result of interference between reflections from both its front and back edges. They showed that the two edge reflections present different signal features and they present a new strategy that considers the extraction of two edge reflection signal embedded in overall reflection signal, enabling an accurate and quantitative defect characterization.

Tenenbaum, Stutz and Fernandes (2011) carried out a comparison of vibration and wave propagation approaches to assess damage in Euler-Bernoulli beams. Their results with different damage scenarios showed that the vibrational approach has the advantage of being directly applicable in more complex structures. Otherwise, the wave approach has a significant economy of time and computational effort.

Ryue et al. (2011) used the phenomenon of reflection and transmission associated with the presence of a discontinuity for localization and measurement of defect. They analysed non-uniformities by a combined spectral element and finite element method at low frequencies and a combined spectral super element and finite element method at high frequencies, showing an application in rails. They estimated wave reflection and transmission at frequencies between 20 and 40 kHz, showing the feasibility of the approach for realistic waveguides.

Ostachowicz et al. (2012) realized numerical calculations with the Spectral Finite Element Method in one-dimensional structural elements like rods and beams. The results of numerical simulations were compared with experimental measurements employing laser-scanning vibrometry, showing the effectiveness of that method.

Vasques (2013) carried out a theoretical study on wave propagation in one-dimensional structures, and analysed the effects of structural discontinuities on wave motion. He studied the scattering of energy when a wave interacts with damage which is characterised by reflection and transmission coefficients. He analysed two situations, with longitudinal and flexural waves, with two types of damage.

Larico et al. (2013) developed a method for the detection of corrosion by mass loss in an aluminium strip, using Lamb waves in the pitch catch configuration and a signal correlation based technique. This technique compares the measured signal with damage and without damage, however it does not allow for the detection or differentiation of minor damage by mass loss. A refinement of this technique was presented for improving the ability to distinguish between damages of small mass loss.

1.4 Objectives

The specific objectives of this dissertation are to:

- Develop a wave propagation model of a one-dimensional guided structure with symmetric damage in the time and the frequency domain, incorporating a piezoelectric actuator and sensors to detect reflected and transmitted waves.
- Analyse the effects of the size of actuator, the size of the sensor, and the size of symmetric damage in a one-dimensional guided structure, both in the frequency and the time domains.
- Analyse the reflected and transmitted waves, determining which of these waves is better for the identification of damage.

1.5 Contributions

The contribution of this dissertation are as follows:

- From the analysis of scattering longitudinal and flexural waves from a symmetrically part of the beam damaged, it is shown that there is different behaviour of the reflected (or transmitted) longitudinal waves in comparison to flexural waves.
- From the analysis of piezoelectric elements in a guided structure, it is shown that for longitudinal and flexural waves there are optimum lengths of the PZT element to excite the structure as well as lengths of the PZT elements to avoid, when they cannot excite the structure.
- From the analysis of the complete system with optimal parameters, it is shown that for high frequency waves, longitudinal waves are more sensitive than flexural waves, and the pulse-echo configuration is better than the pitch-catch configuration to determine symmetric damage in a beam.

1.6 Outline of the dissertation

The chapters in this dissertation are structured as follows:

In chapter 1 the background is presented, which sets the general scope of the dissertation. The concepts of Structural Health Monitoring and wave propagation are reviewed, together with a literature review, objectives, contributions and the outline.

In chapter 2 the theory about elastic wave propagation applied in guided structures is briefly reviewed and the effects of the symmetric damage in a guided structure with longitudinal and flexural waves are investigated.

In chapter 3 the models of the actuator and sensor are described. Using these models, the optimum length of a PZT element as a function of frequency are analysed.

In chapter 4 the detection and quantification of symmetric damage in a beam are analysed in the time domain, using the combined model of the damage, the PZT actuator and sensor. Longitudinal and flexural waves for pulse-echo and pitch-catch configuration are studied.

Chapter 5 presents the main conclusions from the dissertation. It includes a summary and proposals for further work.

2 WAVE MODEL OF A BEAM CONTAINING SYMMETRIC DAMAGE

2.1 Introduction

The aim of this chapter is to review briefly the theory of wave propagation applied to bars and beams, and the way in which waves are scattered due to symmetric damage. The model is then used to study the effects of the damage in an infinite aluminium beam.

Euler Bernoulli theory is used for flexural analysis, and each bar or beam is described without the inclusion of damping.

2.2 Wave Propagation in bars and beams

Wave propagation is the transport of energy in space and time (DOYLE, 2009). The types of waves of interest are longitudinal and flexural waves which are described in the next section.

2.2.1 Longitudinal waves in bars

Longitudinal waves in bars are a simple case of elastic wave motion. The deformation of a bar in this case is shown in Figure 1 In this case the bar is considered long and slender and is assumed that the stress is uniformly distributed throughout the cross-section. The waves that travel in the bar are characterised by the displacement of the medium, which is parallel to the direction of wave propagation.

Figure 1 - Deformation pattern of longitudinal wave in a bar (transverse displacement greatly exaggerated)

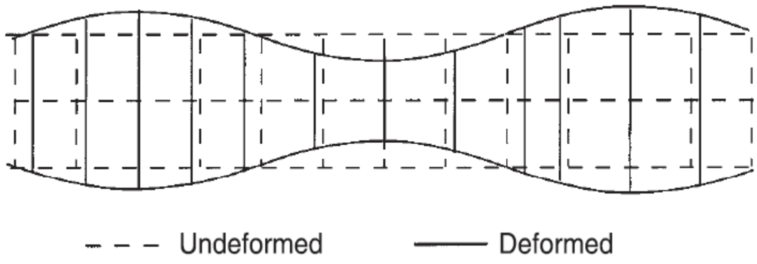

Source: Fahy and Gardonio (2007).

The axial displacement $u(x,t)$ of a bar for free vibration is governed by the partial differential equation (GRAFF, 1975)

$$ES\frac{\partial^2 u}{\partial x^2} - \rho S\frac{\partial^2 u}{\partial t^2} = 0\,, \tag{2.1}$$

where E is the modulus of elasticity, S is the cross-sectional area and ρ is the density of the bar. It is assumed that the vibration of the structure is linear and time-harmonic. This last assumption allows $e^{+i\omega t}$ time dependency to be supressed for clarity, where ω is a circular frequency and $i = \sqrt{-1}$.

A general solution of equation 2.1 for in-plane displacement is given by

$$u(x) = A_l e^{+ik_l x} + A_r e^{-ik_l x}\,, \tag{2.2}$$

where A_l and A_r are the amplitude of propagating longitudinal waves, whose values are given by the boundary conditions and $k_l = \omega/c_l$ is the longitudinal wave number which has units of rad/m. The wavenumber can be thought of as spatial frequency in which k_l is 2π times the number of spatial cycles per unit distance; $c_l = \sqrt{E/\rho} = f\lambda_l$ is the phase velocity with units of m/s (ADAMS, 2007), where f is the frequency in Hz and λ_l is the longitudinal wavelength with $\lambda_l = 2\pi/k_l$. When the phase velocity is constant with respect to frequency, such as this case, they are non-dispersive waves. That is, at each different position in space, the wave maintains its shape.

In equation (2.2), the left-going wave is given by

$$u^-(x) = A_l e^{+ik_l x}\,, \tag{2.3a}$$

and right-going wave is given by

$$u^+(x) = A_r e^{-ik_l x}\,. \tag{2.3b}$$

2.2.2 Flexural waves in beams

Flexural waves in beams travel with a wave motion, which is transverse to the direction of propagation as shown in Figure 2 for infinite uniform Euler-Bernoulli beam. The beam is assumed to have no damping and the effects of rotary inertia and shear stiffness are neglected.

The limitation of the Euler Bernoulli beam model is that it can provide an accurate result only when the ratio of wavelength to thickness is greater than 6 (FAHY; GARDONIO, 2007).

Figure 2 - Deformation pattern of flexural wave in a beam

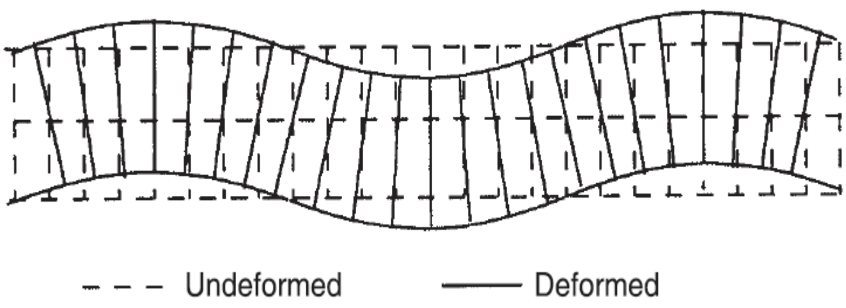

Source: Fahy and Gardonio (2007).

The transverse displacement $w(x,t)$ of the beam is governed by the partial differential equation (GRAFF, 1975)

$$EI\frac{\partial^4 w}{\partial w^4} - \rho S\frac{\partial^2 w}{\partial t^4} = 0 \ , \qquad (2.4)$$

where I is the cross-sectional second moment of area. For a rectangular beam $I = bh^3/12$, where b is the breadth and h is the depth of the beam respectively. As with the case of longitudinal waves, it is assumed that the vibration of the structure is linear and time-harmonic.

The general solution of equation (2.4) for the out-of-plane displacement is given by

$$w(x) = A_1 e^{+k_f x} + A_2 e^{-k_f x} + A_3 e^{+ik_f x} + A_4 e^{-ik_f x} , \qquad (2.5)$$

where A_3 and A_4 are the amplitudes of propagating flexural waves; A_1 and A_2 are evanescent or near-field waves, $k_f = \omega/c_f$ is the flexural wavenumber with units of rad/m. It can be thought of as a spatial frequency; i.e., k_f is related to the number of wavelengths per unit distance, in which $c_F = \omega^{1/2}\left(EI/(\rho S)\right)^{1/4} = f\lambda_f$ is the phase velocity with units of m/s (ADAMS, 2007), where f is the frequency in Hz and λ_f is the flexural wavelength with $\lambda_f = 2\pi/k_f$.

In equation (2.5), the left-going wave is given by

$$w_-(x) = A_1 e^{+k_f x} + A_3 e^{+ik_f x}, \tag{2.6a}$$

and the right-going wave is given by

$$w_+(x) = A_2 e^{-k_f x} + A_4 e^{-ik_f x}. \tag{2.6b}$$

2.2.2.1 Dispersion of Flexural Waves

Flexural waves have a different behaviour compared to longitudinal waves. This is illustrated in Figure 3.

For longitudinal waves, the wave packet travels from position 1 to position 2 maintaining the same shape as shown in Figure 3a.

For flexural waves, the wave packet changes its shape as shown in Figure 3b, the reason for the different shape of this packet wave in the two cases is because the phase velocity for a longitudinal wave depends only on material properties, but in the case of a flexural wave, it varies with frequency.

The use of wave packets such as a tone bursts is important in the study of dispersion in structures. They consist of a group of waves with a carrier frequency, whose amplitude is modulated with a window function such as a Hanning Window (GIURGIUTIU, 2008).

2.2.2.2 Group velocity

The group of velocity is the velocity at which the envelope of the wave packet propagates. In the case of a longitudinal wave the group velocity c_{gl} is equal to the phase velocity c_l. This can be seen in Figure 3c.

In case of the flexural wave, which is dispersive, the wave packet travels at different velocity to that of the phase velocity of the individual waves in the packet. The velocity with which the wave packet propagates in the beam is the group velocity c_{gF}, which is given by (GIURGIUTIU, 2008).

$$c_{gF} = \frac{d\omega}{dk} = 2\left(\frac{EI}{\rho S}\right)^{1/2} k_f . \tag{2.7}$$

For flexural waves, the group velocity is thus twice the phase velocity i.e.:

$$c_{gF} = 2c_F . \tag{2.8}$$

The difference between the phase velocity and group velocity is shown in Figure 3d.

Figure 3 - Diagram of the beam excited by 100 kHz Hanning-windowed signal and its response in the time domain (a) and (c) for longitudinal wave, and (b) and (d) for flexural wave.

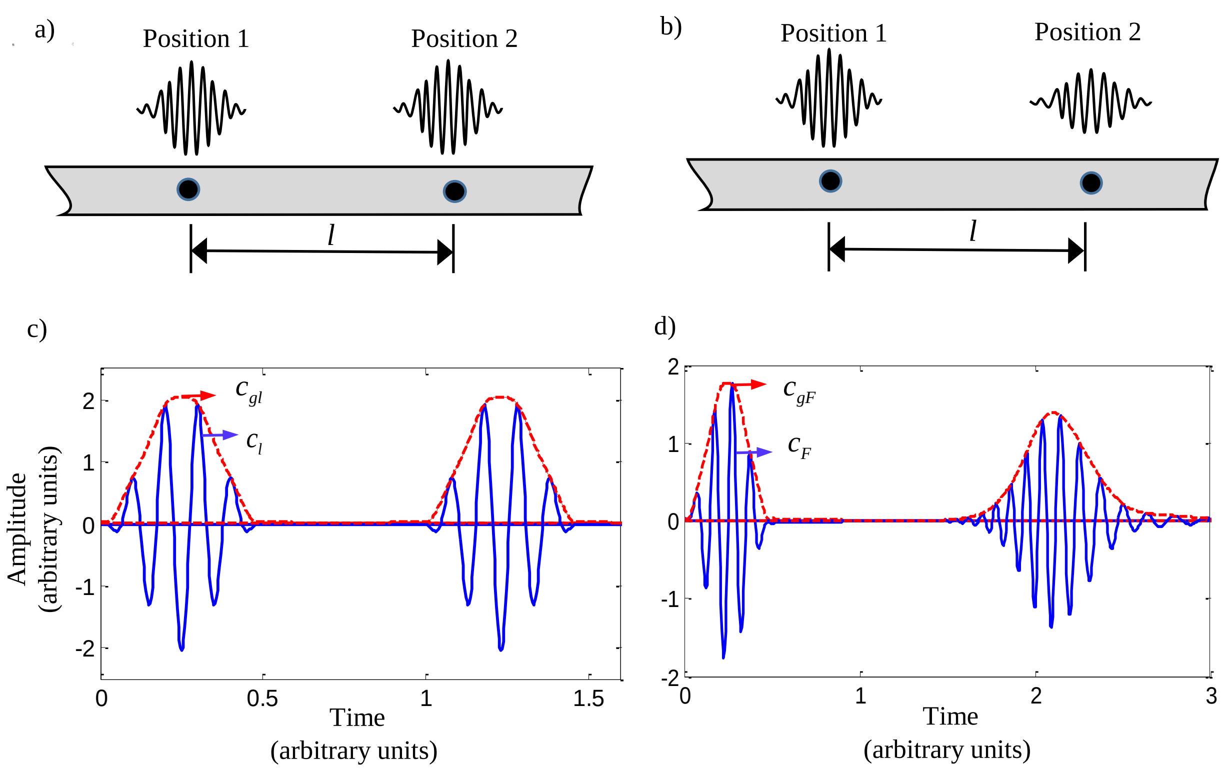

Source: Elaborated by the author.

2.3 Modelling Symmetric Damage

In this dissertation, the damage in an Euler-Bernoulli beam is represented by a symmetric discontinuity, which involves a change in cross-section of the beam. This change could occur in practice by corrosion, for example. Because of this symmetric condition, there is no scattering between longitudinal and flexural waves and vice versa. An incident longitudinal wave will scatter into transmitted and reflected longitudinal waves and an incident flexural wave will scatter into reflected and transmitted near-field and propagating waves. In Figure 4 the position of the damaged section of length l_D in the infinite beam/bar is shown.

Figure 4 - Diagram of the beam/bar structure.

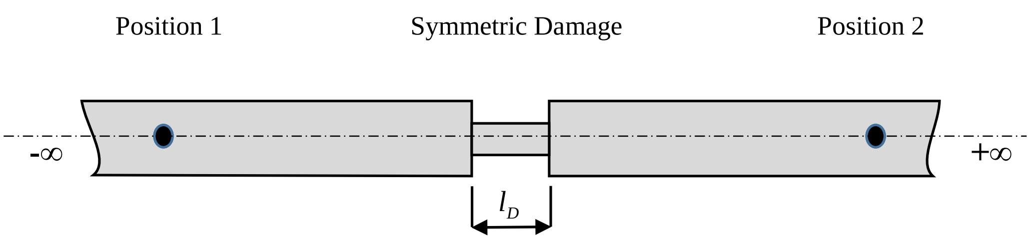

Source: Elaborated by the author.

2.3.1 Interaction of longitudinal waves with the symmetric damage

The decrease of mass and stiffness of the damage of length l_D has an effect on the amplitudes of the reflected and transmitted waves. Figure 5 shows details of the damage and illustrates the incident wave A_{Lr}, the reflected wave A_{Ll} and the transmitted wave A_{Rr}.

Figure 5 - Diagram of the scattering waves for a longitudinal incident wave in a symmetric damage.

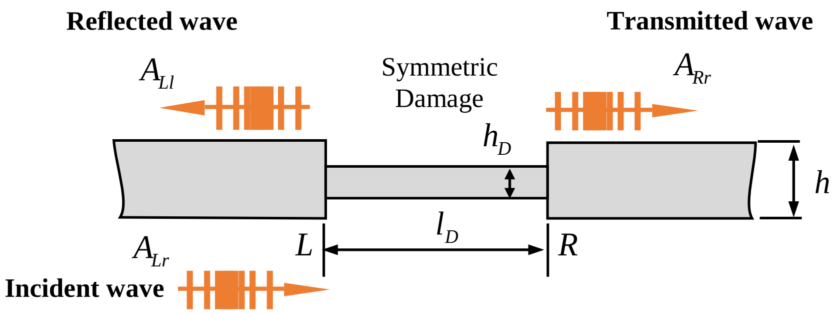

Source: Elaborated by the author.

The approach used by Brennan (1994) to model a PZT actuator attached to a beam is adopted here to model the damage. Uniform sections of the beam are modelled as waveguides, which can be represented by simple wave transmission matrices. The part of the beam with the section changed (the damage) is considered as another uniform beam element. The state vectors at each side of the junction are used to connect the beam elements together. The sections of the beam either side of the damage are considered semi-infinite to avoid reflected waves at boundaries.

The relationship between the state vector and the waves at a junction is given by Brennan (1994)

$$\begin{Bmatrix} u \\ F \end{Bmatrix} = \begin{Bmatrix} u \\ ESu' \end{Bmatrix} = \begin{bmatrix} 1 & 1 \\ iESk_l & -iESk_l \end{bmatrix} \begin{Bmatrix} A_l \\ A_r \end{Bmatrix}, \tag{2.9}$$

where $'$ denotes the spatial derivate with respect to x and F is the internal in-plane force. Equation (2.9) can be written for the two junctions either side of the damage as

$$\mathbf{h}_B^L = \mathbf{H}_B \mathbf{a}_B^L \tag{2.10}$$

and

$$\mathbf{h}_B^R = \mathbf{H}_B \mathbf{a}_B^R, \tag{2.11}$$

where $\mathbf{h}_B = \{u \quad F\}^T$ is the state vector, $\mathbf{H}_B$ is the transformation matrix in equation (2.9) and $\mathbf{a}_B = \{A_l \quad A_r\}^T$ is the vector of waves. The subscript B indicates that the variable belongs to the beam, the superscripts L and R are the left- and right –hand junctions and the superscript T denotes the transpose. The corresponding relationship for two junctions at each ends of the damage are given by

$$\mathbf{h}_D^L = \mathbf{H}_D \mathbf{a}_D^L \tag{2.12}$$

and

$$\mathbf{h}_D^R = \mathbf{H}_D \mathbf{a}_D^R, \tag{2.13}$$

where in this case the subscript D denotes that these equations belong to the damaged section. Force balance and continuity conditions at the junctions can be applied, so, the state vectors of the junctions on the beam side without damage are equal to the state vectors of the junctions on the damaged section of the beam, so that

$$\mathbf{H}_B \mathbf{a}_B^L = \mathbf{H}_D \mathbf{a}_D^L \tag{2.14}$$

and

$$\mathbf{H}_B\mathbf{a}_B^R = \mathbf{H}_D\mathbf{a}_D^R. \qquad (2.15)$$

The relationship between the wave vectors $\mathbf{a}_D^L$ and $\mathbf{a}_D^R$ is given by

$$\mathbf{a}_D^R = \mathbf{T}_D\mathbf{a}_D^L, \qquad (2.16)$$

where $\mathbf{T}_D$ is the spatial transformation matrix for the damaged section of the beam and is given by

$$\mathbf{T}_D = \begin{bmatrix} e^{jk_l l_D} & 0 \\ 0 & e^{-jk_l l_D} \end{bmatrix}, \qquad (2.17)$$

Substituting equations (2.14) and (2.15) into (2.16) gives

$$\mathbf{H}_B\mathbf{a}_B^R - \mathbf{H}_D\mathbf{T}_D\mathbf{H}_D^{-1}\mathbf{H}\mathbf{a}_B^L = 0. \qquad (2.18)$$

This is a relationship between the waves either side of the damage and it can be rearranged to group the waves into incoming and outgoing waves, obtaining a simplified system given by

$$\mathbf{a}_{\mathrm{out}} = \mathbf{C}^{-1}\mathbf{B}\mathbf{a}_{\mathrm{in}}, \qquad (2.19)$$

where

$$\mathbf{a}_{\mathrm{in}} = \begin{Bmatrix} A_{Rl} \\ A_{Lr} \end{Bmatrix}, \qquad (2.20)$$

$$\mathbf{a}_{\mathrm{out}} = \begin{Bmatrix} A_{Ll} \\ A_{Rr} \end{Bmatrix}, \qquad (2.21)$$

and the matrices **B** and **C** are given by

$$\mathbf{B} = \left[\left(\mathbf{H}_B\right)_1 \middle| \; \left(\mathbf{H}_D\mathbf{T}_D\mathbf{H}_D^{-1}\mathbf{H}_B\right)_2 \right] \qquad (2.22)$$

and

$$\mathbf{C} = \left[\left(\mathbf{H}_D \mathbf{T}_D \mathbf{H}_D^{-1} \mathbf{H}_B \right)_1 \middle| \quad \left(\mathbf{H}_B \right)_2 \right], \tag{2.23}$$

where the subscripts 1 and 2 denote the columns of the respective matrices.

2.3.1.1 Simulations

In this section the effect of damage on a longitudinal incident wave is investigated on a bar/beam with the properties given in Table 1. The ratio of the transmitted wave to the incident wave $\left(A_{Rr}/A_{Lr}\right)$ and the ratio of the reflected wave to the incident wave $\left(A_{Ll}/A_{Lr}\right)$ are obtained, for different damage lengths and/or different frequencies which are represented in non-dimensional form l_D/λ_l . The results are shown in Figure 6.

Table 1 - Material and geometric properties of the beam

Material and geometric properties of the beam			
Property	**symbol**	**value**	**units**
Density	ρ	2370	Kg/m^3
Young's Modulus	E	71x10^9	N/m^2
Beam width	b	14	mm
Thickness	h	2	mm

Source: Elaborated by the author.

It can be seen from Figure 6 that the maximum amplitude of the reflected wave and the minimum value of the transmitted wave occurs when

$$\frac{l_D}{\lambda_l} = \frac{2n-1}{4} \qquad n = 1, 2, 3... \tag{2.24}$$

The maximum reflected wave increases when the damage increases. The incident wave is totally transmitted when

$$\frac{l_D}{\lambda_l} = \frac{n}{2}. \tag{2.25}$$

Thus, if the frequency of the incident longitudinal wave is such that a longitudinal wavelength is half that of the length of the damage, then this wave will be "blind" to any damage in the beam. Note that the maxima, minima of wave reflection and total wave transmitted occur at the same frequency independent of the degree of damage.

Figure 6 - Reflected and transmitted propagating longitudinal waves due to an incident propagating longitudinal wave for different percentages of symmetric damage; Solid blue line —, 0% damage; dashed red line ---, 10% damage; thick dotted green line ····, 30% damage; dashed dot cyan line −·−, 50% damage.

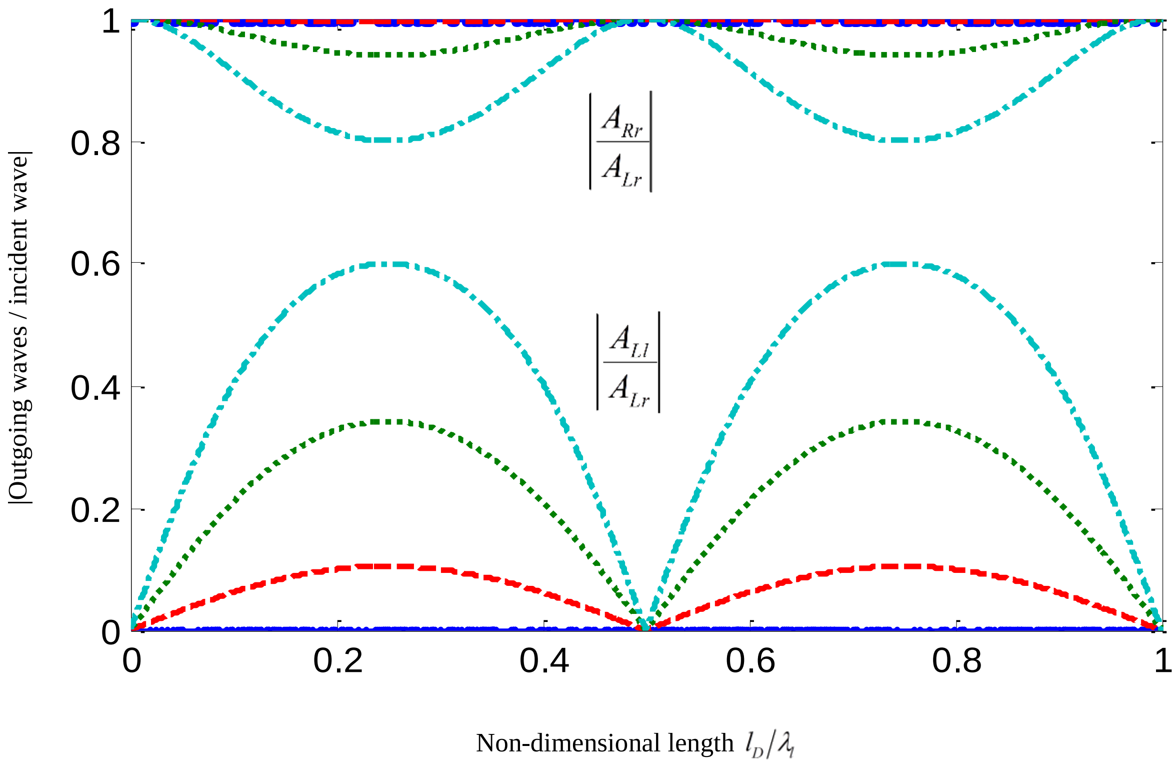

Source: Elaborated by the author.

2.3.2 Interaction of Flexural waves with the symmetric damage

As with the longitudinal wave analysis, the decrease of mass and stiffness, of this symmetric damage of length l_D in a beam, has an effect on the amplitudes of the scattered waves. However, in this case, there are near-field waves in addition to propagating waves. Figure 7 shows details of the damage and illustrates the incident wave A_{L4}, the reflected propagating wave A_{L3}, the reflected near-field wave A_{L1}, the transmitted propagating wave A_{R4} and the transmitted near-field wave A_{R2}.

Figure 7 - Diagram of the scattering waves for a flexural incident wave

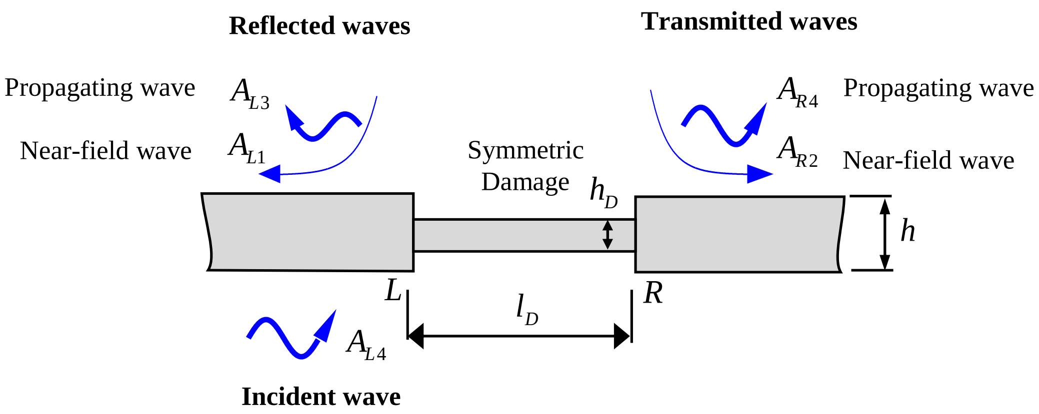

Source: Elaborated by the author.

As with longitudinal waves, there is a relationship between the state vector and the waves at a junction. It is given by Brennan (1994)

$$\begin{Bmatrix} w \\ \theta \\ M \\ Q \end{Bmatrix} = \begin{Bmatrix} w \\ w' \\ EIw'' \\ EIw''' \end{Bmatrix} = \begin{bmatrix} 1 & 1 & 1 & 1 \\ k_f & jk_f & -k_f & -jk_f \\ EIk_f^2 & -EIk_f^2 & EIk_f^2 & -EIk_f^2 \\ EIk_f^3 & -jEIk_f^3 & -EIk_f^3 & jEIk_f^3 \end{bmatrix} \begin{Bmatrix} A_1 \\ A_3 \\ A_2 \\ A_4 \end{Bmatrix}, \tag{2.26}$$

where θ is the beam rotation, M is the internal bending moment and Q is the internal out-of-plane force. Equation (2.26) can be written for the two junctions at the side without damage as

$$\mathbf{v}_B^L = \mathbf{V}_B \mathbf{a}_B^L \tag{2.27}$$

and

$$\mathbf{v}_B^R = \mathbf{V}_B \mathbf{a}_B^R, \tag{2.28}$$

where $\mathbf{v}_B = \{w \quad \theta \quad M \quad Q\}^T$ is the state vector, $\mathbf{V}_B$ is the transformation matrix in Equation (2.26) and $\mathbf{a}_B = \{A_1 \quad A_3 \quad A_2 \quad A_4\}^T$ is the vector of waves. As with the longitudinal case, force balance and continuity conditions at the junctions can be applied, which results in a similar equation to (2.19), but in this case, it is given by

$$\mathbf{V}_B \mathbf{a}_B^R - \mathbf{V}_D \mathbf{T}_D \mathbf{V}_D^{-1} \mathbf{V}_B \mathbf{a}_B^L = 0, \tag{2.29}$$

where

$$\mathbf{T}_D = \begin{bmatrix} e^{k_{fD}l_D} & 0 & 0 & 0 \\ 0 & e^{jk_{fD}l_D} & 0 & 0 \\ 0 & 0 & e^{-k_{fD}l_D} & 0 \\ 0 & 0 & 0 & e^{-jk_{fD}l_D} \end{bmatrix},$$

and k_{fD} is the flexural wavenumber of the beam with damage. Note that in the longitudinal case the wavenumber in the damaged section of the beam is the same as in the undamaged case, but in the flexural case this is not so. In the same way as for the longitudinal case, it is possible to group the waves into incoming and outgoing waves given by

$$\mathbf{a}_{\text{out}} = \mathbf{C}^{-1}\mathbf{B}\mathbf{a}_{\text{in}}, \tag{2.30}$$

where the vector of wave amplitudes is given by

$$\mathbf{a}_{\text{in}} = \begin{Bmatrix} A_{R1} \\ A_{R3} \\ A_{L2} \\ A_{L4} \end{Bmatrix} \tag{2.31}$$

and

$$\mathbf{a}_{\text{out}} = \begin{Bmatrix} A_{L1} \\ A_{L3} \\ A_{R2} \\ A_{R4} \end{Bmatrix}, \tag{2.32}$$

and the matrices **B** and **C** are given by

$$\mathbf{B} = \left[\left(\mathbf{V}_B\right)_1 \middle| \; \left(\mathbf{V}_B\right)_2 \middle| \; \left(\mathbf{V}_D\mathbf{T}_D\mathbf{V}_D^{-1}\mathbf{V}_B\right)_3 \middle| \; \left(\mathbf{V}_D\mathbf{T}_D\mathbf{V}_D^{-1}\mathbf{V}_B\right)_4 \right] \tag{2.33}$$

and

$$\mathbf{C} = \left[\left(\mathbf{V}_D\mathbf{T}_D\mathbf{V}_D^{-1}\mathbf{V}_B\right)_1 \middle| \; \left(\mathbf{V}_D\mathbf{T}_D\mathbf{V}_D^{-1}\mathbf{V}_B\right)_2 \middle| \; \left(\mathbf{V}_B\right)_3 \middle| \; \left(\mathbf{V}_B\right)_4 \right], \tag{2.34}$$

where the subscripts 1 - 4 denote the columns of the respective matrices.

2.3.2.1 Simulations

In this section, the effect of damage on a flexural incident wave is investigated on a beam with the properties given in Table 1. The ratio of the reflected wave to the incident wave $\left(A_{L3}/A_{L4}\right)$ and the ratio of the transmitted wave to the incident wave $\left(A_{R3}/A_{L4}\right)$ are obtained, for different frequencies which are represented in non-dimensional form l_D/λ_f . The near-field waves are not considered in this analysis because they decay rapidly away from the boundaries of the damage. However, they were important for the development of the model studied in this section.

The results are shown in Figure 8. It can be observed that the value maximum of the reflected wave corresponds to different ratios of l_D/λ_f , when the damage increases. This is because the wavespeed is a function of the thickness of the beam, unlike that for longitudinal waves. For the rectangular beam shown in Figure 7, the wavespeed is given by $c_F = \left(Eh^2/(12\rho)\right)^{1/4}\omega^{1/2}$ so that when the thickness of the damages section reduces, so does the wavespeed. This can have important implications when using waves to detect a reduction in beam thickness, and this is discussed in the chapter 4.

Figure 8 - Reflected and transmitted propagating flexural waves due to an incident propagating flexural wave for different percentages of symmetric damage; Solid blue line —, 0% damage; dashed red line ---, 10% damage; thick dotted green line ····, 30% damage; dashed dot cyan line −·−, 50% damage.

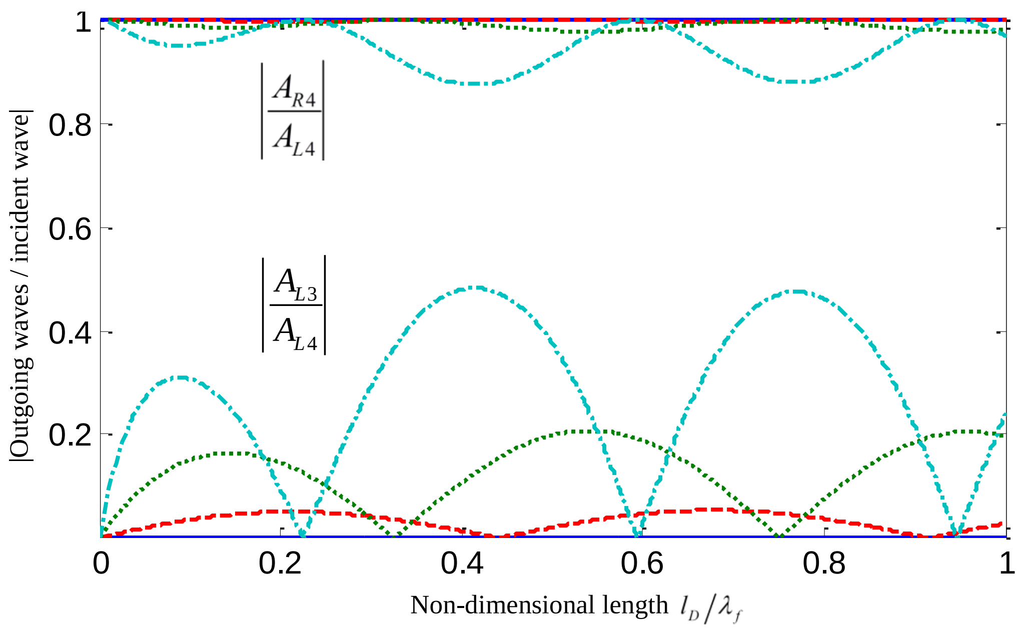

Source: Elaborated by the author.

2.4 Conclusions

In this chapter, longitudinal and flexural wave theory in bars and beams has been briefly reviewed. A model has then been developed to investigate the way in which these waves interact with damage that is symmetric with respect to the neutral axis.

For both types of waves there is scattering that is dependent on frequency. For longitudinal waves is found that the maxima and minima of wave reflection and wave transmission occurs at the same frequency independent of the degree of damage. However, for flexural waves, the situation is different; the maxima and minima of wave reflection and total wave transmitted occur at different frequencies depending upon the degree of damage. Further, it is found that due to the dispersive nature of bending waves, it is possible for the reflected wave amplitude to decrease rather than increase as the beam thickness is reduced.

3 COUPLING ACTUATORS AND SENSORS TO A WAVE MODEL OF A BEAM

3.1 Introduction

The theory of wave propagation, reviewed in chapter 2 is used in this chapter to model the sensors and actuator acting on an Euler-Bernoulli beam. Both longitudinal and flexural waves are considered. The type of piezoelectric material used in this dissertation is the PZT (lead zirconate titanate); it can be used as actuator as well as sensor.

Brennan (1994) analysed these models, theoretical and experimentally, considering their dynamic effects of mass and stiffness with application to active control.

The models are used in this chapter to investigate the optimum lengths of actuator and sensor compared to a wavelength.

3.2 Piezoelectric Actuator

Piezoelectric actuators come in many geometric and material configurations. The most common configuration is a unimorph, using only one PZT element bonded to one side of the structure, generating longitudinal and flexural waves simultaneously. Another configuration is the bimorph, which uses two PZT elements, one either side of the structure, generating longitudinal and flexural waves separately. A bimorph configuration is considered in this dissertation, which is perfectly bonded to opposite sides of a beam.

3.2.1 Longitudinal vibration actuator

The bimorph actuator is shown in Figure 9. If the PZT elements are driven in phase, they work as a longitudinal vibration actuator and generate axial forces at the end of the elements.

Figure 9 - Diagram of the Actuator, generating longitudinal waves.

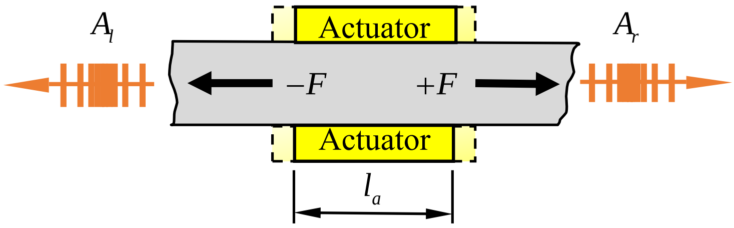

Source: Elaborated by the author.

3.2.1.1 Static Model of the actuator - The Strain Energy Model

This model was developed by Wang and Rogers (1991), being especially used in the cases where the beam thickness is large compared with the actuator thickness. The equation that relates the induced force F to the applied voltage for the two actuators is given by

$$\frac{F}{V_{in}} = \frac{2Ebd_{31}}{6\hat{d} + \psi}, \tag{3.1}$$

where $\hat{d} = h_p / h$, $\psi = Eh/(E_p h_p)$, d_{31} is the piezoelectric constant, h_p and E_p are the thickness and the Young's modulus of the PZT elements, respectively, V_{in} is the input voltage, b and h are the width and the thickness of the beam, respectively.

3.2.1.2 Waves generated by the PZT longitudinal actuators

Left and right going longitudinal waves generated by the bimorph actuator showed in Figure 9 are given by Brennan (1994)

$$\begin{Bmatrix} A_l \\ A_r \end{Bmatrix} = \frac{-j}{2ESk_l} \begin{bmatrix} 1 & e^{-jk_l l_a} \\ 1 & e^{jk_l l_a} \end{bmatrix} \begin{Bmatrix} -F \\ F \end{Bmatrix}, \tag{3.2}$$

where l_a is the length of the actuator. Using Equation (3.2), the properties of the beam given in Table 1 and the properties of the PZT element given in Table 2, the longitudinal displacement as a function of a non-dimensional length l_a / λ_l is shown in Figure 10. It can be seen that as frequency increases (λ_l becomes smaller), the longitudinal displacement diminishes when the length of the actuator equals an integer multiple of a longitudinal wavelength. At this frequency the actuators cannot excite the structure.

Table 2 – Material and geometric properties of the piezoelectric

Material and geometric properties of the piezoelectric elements			
Property	**symbol**	**value**	**units**
Young's Modulus	E_p	$66x10^9$	N/m^2
Piezoelectric constant	d_{31}	$-190x10^{-12}$	m/v
Capacitance	c	$430x10^{-9}$	F
Width	b_p	14	mm
Thickness	h_p	0.19	mm

Source: Elaborated by the author.

Figure 10 - Influence of the ratio of length of actuator with wavelength on the longitudinal displacement per voltage, for longitudinal vibration actuators.

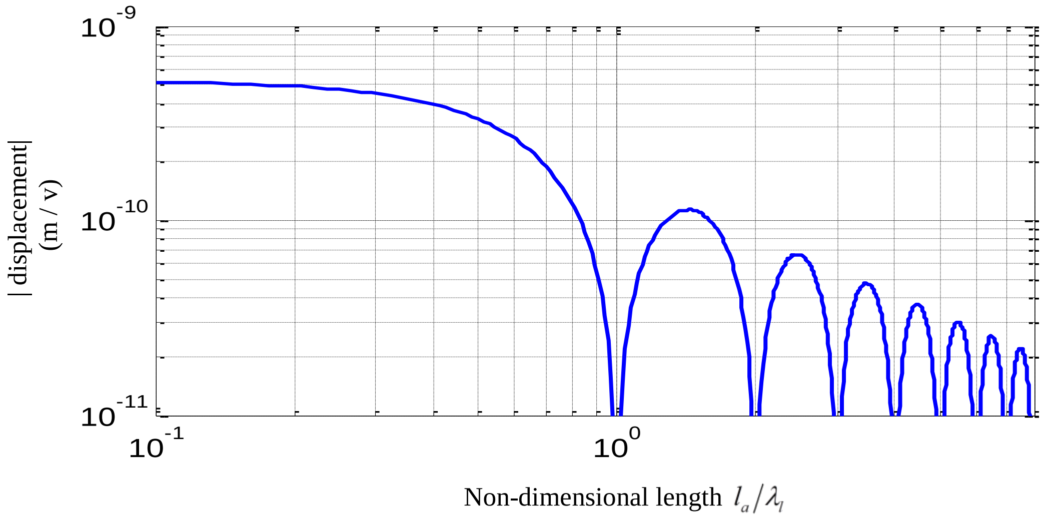

Source: Elaborated by the author.

3.2.2 Flexural vibration actuator

If the PZT elements are driven in anti-phase, they work as a flexural vibration actuator and generate moments at the ends of elements. The bimorph actuator is shown in Figure 11.

Figure 11 - Diagram of the Actuator, generating flexural and evanescent propagating waves.

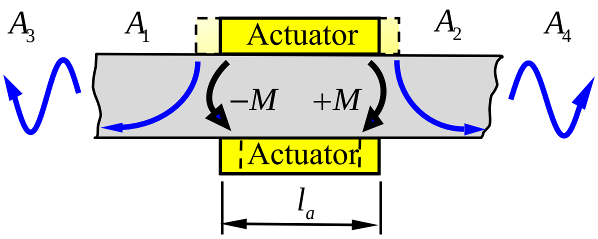

Source: Elaborated by the author.

3.2.2.1 Static Model of the actuator - The Euler Bernoulli model

This model was developed by Crawley and Anderson (1990) and they verified that it has a good approximation with respect to a finite element model. The induced Moment *M* to the applied voltage for the two actuators is given by

$$\frac{M}{V_{in}} = \frac{hEb(1+\hat{d})}{(6\hat{d}+\psi+12\hat{d}^2+8\hat{d}^3)}. \qquad (3.3)$$

3.2.2.2 Waves generated by the PZT flexural actuators

Left and right going propagating flexural and evanescent waves generated by the pair of actuators shown in Figure 11 are given by Brennan (1994)

$$\begin{Bmatrix} A_1 \\ A_2 \\ A_3 \\ A_4 \end{Bmatrix} = \frac{1}{4EIk_f^2}\begin{bmatrix} 1 & e^{-k_f l_a} \\ -1 & -e^{k_f l_a} \\ -1 & -e^{-jk_f l_a} \\ 1 & e^{jk_f l_a} \end{bmatrix}\begin{Bmatrix} -M \\ M \end{Bmatrix}. \qquad (3.4)$$

Similar to longitudinal response, the lateral displacement obtained as a function of a non-dimensional length l_a/λ_f and it is shown in Figure 12, where the solid blue line shows the effect of propagating flexural waves. It can be seen that as frequency increases (λ_f becomes smaller) the lateral displacement diminishes when the length of the actuator equals a multiple integer of the longitudinal wavelength, then the actuators cannot excite the structure.

The dashed red line shows the effect of the propagating flexural waves adding the effect of evanescent flexural waves.

Comparing these plots there is an increase in the lateral displacement. In practice, this is observed close to the actuator because of evanescent waves do not propagate along the beam.

Figure 12 - Influence of the ratio of length of actuator with wavelength on the lateral displacement per voltage for flexural vibration actuators; dashed red line ---, effect of the propagating flexural and evanescent waves; Solid blue line —, effect of the propagating flexural waves.

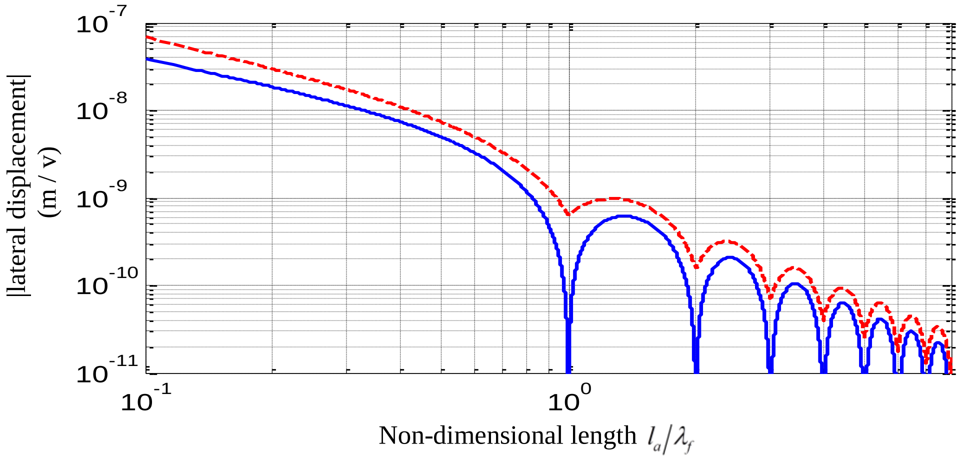

Source: Elaborated by the author

Figure 13 shows the reason why longitudinal and flexural waves cannot be generated by the actuators in the right side of the beam, when the frequency of excitation is such that the length of the actuator is equal to a wavelength. The solid and dashed blue lines are waves generated by the right side and left side of the actuators respectively. It can be seen that they cancel each other and thus the structure is not excited.

Figure 13 - Diagram of the Actuator with no-generating longitudinal waves.

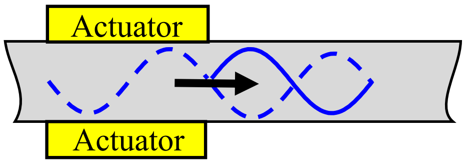

Source: Elaborated by the author.

3.3 Piezoelectric Sensor

In this section expressions are derived for the voltage generated by the longitudinal and flexural sensors due to incident waves. Two piezoelectric elements perfectly bonded to opposite sides of the beam are considered. With this configuration, it is possible to sense flexural and longitudinal effects separately. It is assumed that they have negligible mass and stiffness and the strain is constant across the width of the beam and the sensors.

3.3.1 Longitudinal vibration Sensors

Figure 14 shows a diagram of two sensors on opposite sides of the beam with longitudinal wave incident on the sensor.

Figure 14 - Diagram of the longitudinal wave sensor.

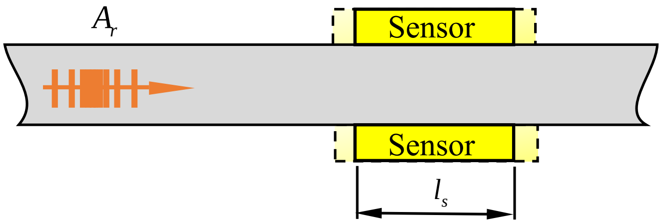

Source: Elaborated by the author

The voltage generated by a sensor is given by Brennan (1994)

$$V_{out} = \frac{d_{31}E_p b_p \left(u^+(l_s) - u^-(0)\right)}{c}, \tag{3.5}$$

where c is the capacitance of the PZT elements, l_s is the length of the sensor and $u^+(l_s) - u^-(0)$ is the difference in the displacements at the ends of the sensor. When a wave is incident on the sensor, this is equal to

$$u^+(l_s) - u^-(0) = A_r\left(1 - e^{-jk_l l_s}\right). \tag{3.6}$$

For a sensor positioned far from an actuator, the ratio of output voltage from the sensor to incident wave amplitude is shown as a function of a non-dimensional length l_s/λ_l in Figure 15. It can be seen that for lengths of sensor equal to multiple integers of the longitudinal wavelength, the output is zero.

Figure 15 - Influence of the ratio of length of sensor with wavelength on the voltage generated for longitudinal sensor.

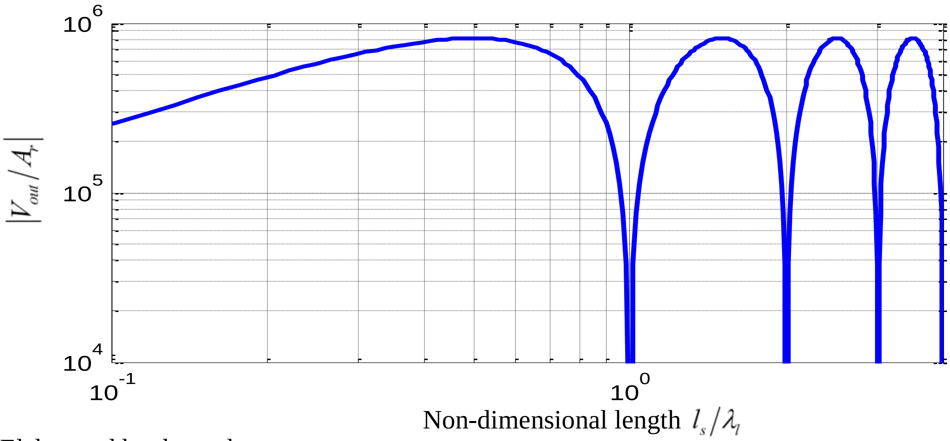

Source: Elaborated by the author

The reason for the output being zero when l_s/λ_l = 1, 2, 3… is because there is no strain in the sensor as illustrated as illustrated in Figure 16.

Figure 16 - Diagram of the sensor with no-sensing longitudinal waves.

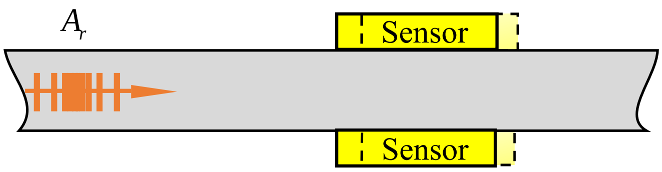

Source: Elaborated by the author.

3.3.2 Flexural vibration Sensors

Figure 17 shows a diagram of two sensors on opposite sides of the beam, with an incident propagating flexural wave.

Figure 17 - Diagram of the sensors, sensing flexural waves, where the dashed black line and red line indicate the motion of the sensors and the slope on that point respectively.

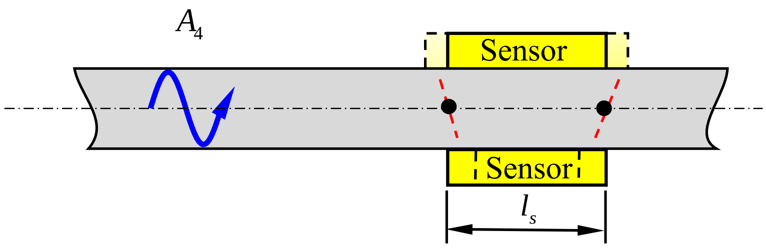

Source: Elaborated by the author.

The voltage generated by a sensor is given by Brennan (1994)

$$V_{out} = \frac{d_{31} h E_p b_p \left(w'_+(l_s) - w'_-(0) \right)}{2c}, \tag{3.7}$$

where the prime denotes the spatial derivate with respect to x and $w'_+(l_s) - w'_-(0)$ is the difference of the slopes at the ends of the sensor, which is given by

$$w'_+(l_s) - w'_-(0) = A_4 j k_f \left(1 - e^{-jk_f l_s} \right). \tag{3.8}$$

As with the longitudinal case, the ratio of output voltage from the sensor to incident wave amplitude is shown as a function of a non-dimensional length l_s/λ_f in Figure 18. It can be seen that the voltage generated has an increasing tendency with frequency and for lengths of sensor equal to multiple integers of the flexural wavelength, the output is zero.

Figure 18 - Influence of the ratio of length of sensor with wavelength on the voltage generated for flexural sensor, dashed red line ---, effect of the propagating flexural and evanescent waves; Solid blue line —, effect of the propagating flexural waves.

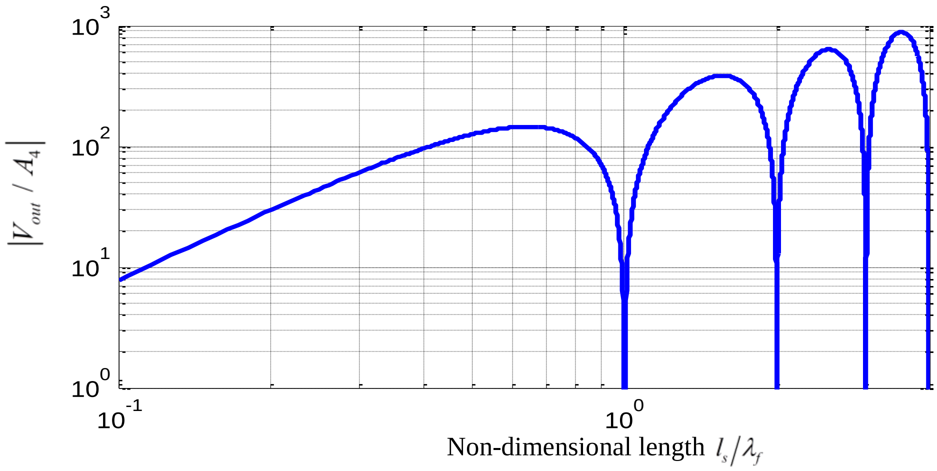

Source: Elaborated by the author.

The reason for the output being zero when l_s/λ_f = 1, 2, 3… for propagating flexural waves is because there is no strain in the sensor as illustrated as illustrated in Figure 19.

Figure 19 - Diagram of the sensors, no-sensing flexural waves, where the dashed black line and red line indicate the motion of the sensors and the slope on that point respectively.

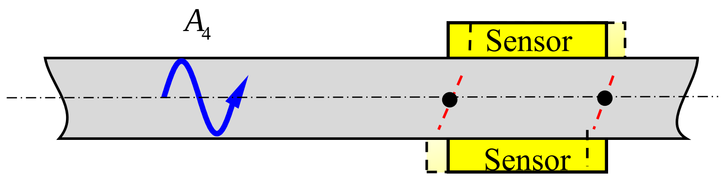

Source: Elaborated by the author.

3.4 Beam with actuator and sensors without damage

In the previous sections sensors and actuators coupled to a beam were analysed separately. In this section a beam with both actuators, sensors in the bimorph configuration are studied. In Figure 20 the arrangement of the PZT elements on the beam is shown. PZT 1 is used as both an actuator and a sensor and the PZT 2 used as a sensor. Note that it is assumed that the actuator and sensor have the same length.

Figure 20 - Diagram showing the model without damage.

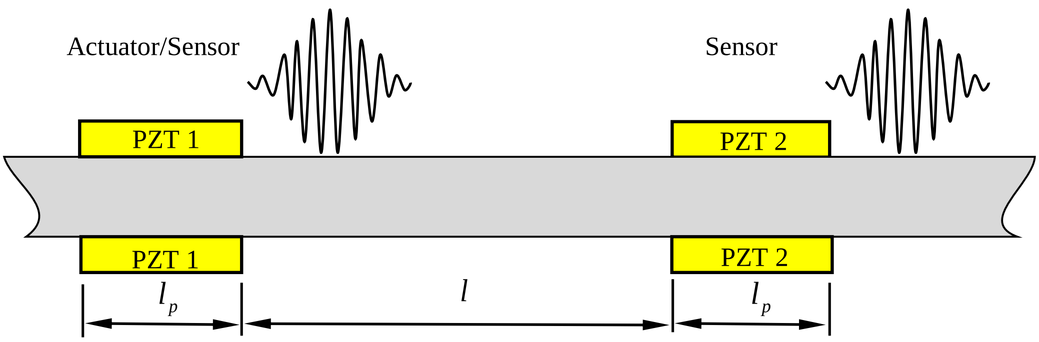

Source: Elaborated by the author.

3.4.1 Longitudinal waves

The response of PZT 1 is obtained by combining equations (3.1), (3.2), (3.5) and (3.6), which is given by

$$\frac{V_{out}}{V_{in}} = \frac{jd_{31}^2 E_p b_p}{h_p k_l c(6+\psi)}\left(e^{-jk_l l_p} - 1\right), \tag{3.9}$$

Where l_p is the length of the PZT element. The response of PZT 2, when $l > 0$, is obtained by combining equations (2.3b), (3.1), (3.2), (3.5) and (3.6), which is given by

$$\frac{V_{out}}{V_{in}} = -\frac{jd_{31}^2 E_p b_p}{2h_p k_l c(6+\psi)}\left(e^{-jk_l l}\right)\left(e^{-jk_l l_p} - 1\right)^2. \tag{3.10}$$

3.4.1.1 Simulation

For the configuration in Figure 20, the input-output relationships are plotted in Figure 21 as a function of l_p/λ_l, using equations (3.9) and (3.10) an the properties given in Tables 1, 2 and a value of *l* = 853mm. It can be seen, only for PZT 2, that the largest responses occur when $l_p/\lambda_l = 1/2$, and no responses are registered when $l_p/\lambda_l = 1$.

Figure 21 - Influence of l_p/λ_l on the Voltage ratio for longitudinal waves; dashed red line ---, PZT1 located at the left side of the beam; Solid blue line —, PZT 2 located at the right side of the beam.

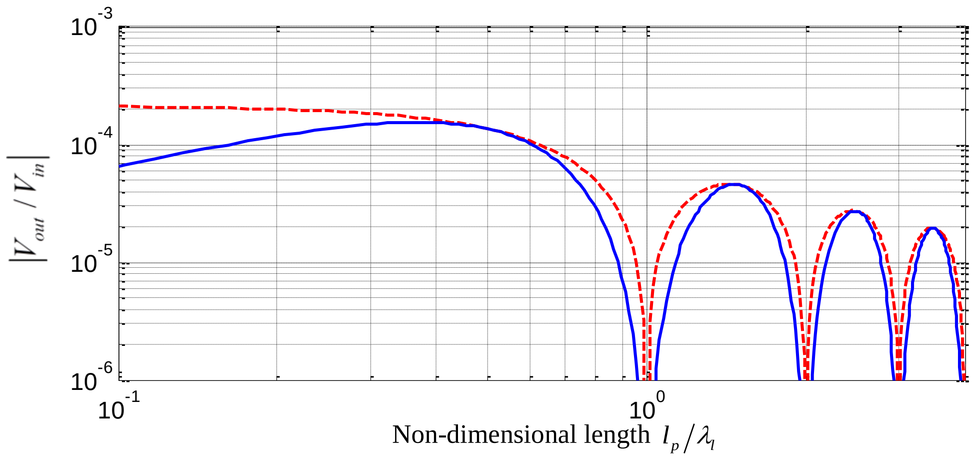

Source: Elaborated by the author.

3.4.2 Flexural waves

The response of PZT 1 is obtained by combining equations (3.3), (3.4), (3.7) and (3.8), which is given by

$$\frac{V_{out}}{V_{in}} = \frac{3d_{31}^2 E_p b_p\left(1+\hat{d}\right)}{2h_p k_f c\left(6+\psi+12\hat{d}+8\hat{d}^{\wedge 2}\right)}\left(\left(1-e^{-k_f l_p}\right) - j\left(1-e^{-jk_f l_p}\right)\right). \tag{3.11}$$

The response of PZT 2, when $l > 0$, is obtained by combining equations (2.6b), (3.3), (3.4), (3.7), (3.8) and neglecting the evanescent component (because the location of PZT 2, which is given by

$$\frac{V_{out}}{V_{in}} = \frac{3jd_{31}^2 E_p b_p \left(1+\hat{d}\right)}{4h_p k_f c\left(6+\psi+12\hat{d}+8\hat{d}^2\right)}\left(\left(e^{-jk_f l}\right)\left(1-e^{-jk_f l_p}\right)^2\right). \qquad (3.12)$$

3.4.2.1 Simulation

These input-output relationships are plotted as a function of l_p/λ_f in Figure 22. Again, as in longitudinal case, it can be seen, for PZT 2, that the largest responses occur when $l_p/\lambda_f = 1/2$ and there are problems when the sensor or actuator is a multiple integer of a wavelength. It can be seen that there are differences between the measurements at PZT 1 and PZT 2 at these frequencies, and this is due to the evanescent waves being present at PZT1 but not at PZT2.

Figure 22 - Influence of l_p/λ_f on the Voltage ratio for flexural waves; dashed red line ---, PZT1 located at the left side of the beam; Solid blue line —, PZT 2 located at the right side of the beam.

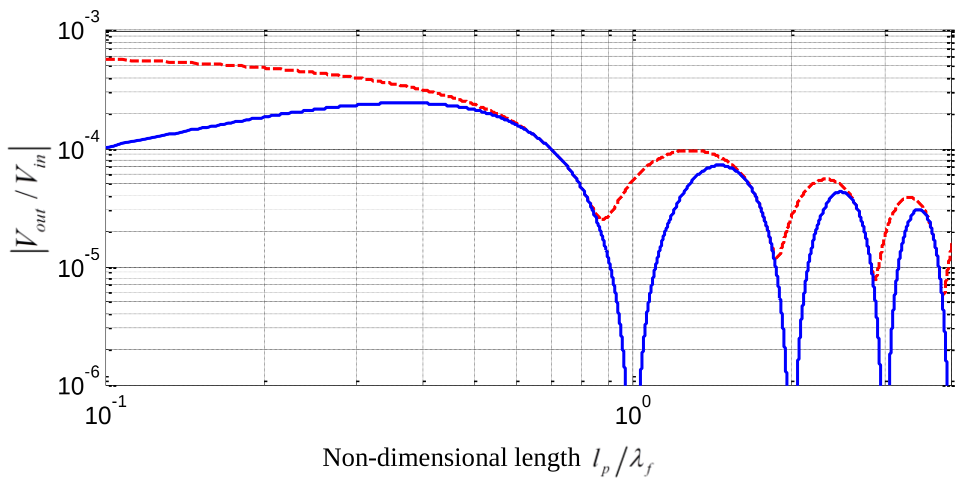

Source: Elaborated by the author.

3.5 Conclusions

This chapter was described models of sensors and actuators coupled to a wave model of a beam, obtaining from the analysis realised, the following conclusions

Mathematical expressions have been obtained, for the actuation and sensing of longitudinal and flexural waves. With these expressions, it has been shown that for a PZT element (actuator or sensor) a good choice of frequency when the length of the PZT element is a half a wavelength. In this case, waves are strongly excited and sensed. When the length of the PZT element equals one wavelength, waves cannot be excited or sensed.

4 IDENTIFICATION OF SYMMETRIC DAMAGE IN A BEAM

4.1 Introduction

In this chapter, the models of an infinite Euler-Bernoulli beam with symmetric damage and piezoceramic patches placed either side of this damage are coupled together. The piezoelectric patches are used in pulse-echo and pitch catch configurations for both longitudinal and flexural waves.

The complete model is developed in the frequency domain, which is then transformed into the time domain using the Inverse Fourier Transform. Simulations are then conduced to investigate the way in which the damage affects wave propagation.

4.2 Configuration for Damage Identification

Figure 23 illustrates the configuration of the beam investigated in this chapter. Note that PZT 1 generates a high frequency wave packet (black line).

In the pulse-echo configuration, PZT 1 is used as both an actuator and a sensor to detect the reflected waves from the damage (blue wave packet).

In the pitch-catch configuration, PZT 1 is used as an actuator and PZT 2 is used as a sensor to detect the wave transmitted beyond the damage (red wave packet).

For the simulations carried out in this section of the dissertation, PZT 1 senses the initial response of the actuator and also senses the reflected wave generated by the damage, and PZT 2 senses only the transmitted waves.

Figure 23 - Illustration of the beam set-up. The black wave packet is generated by PZT 1, the blue wave packet is reflected from the damage section and the red wave packet is transmitted past the damage section. Note that PZT 1 acts as both an actuator and a sensor, and that PZT 2 acts only as a sensor.

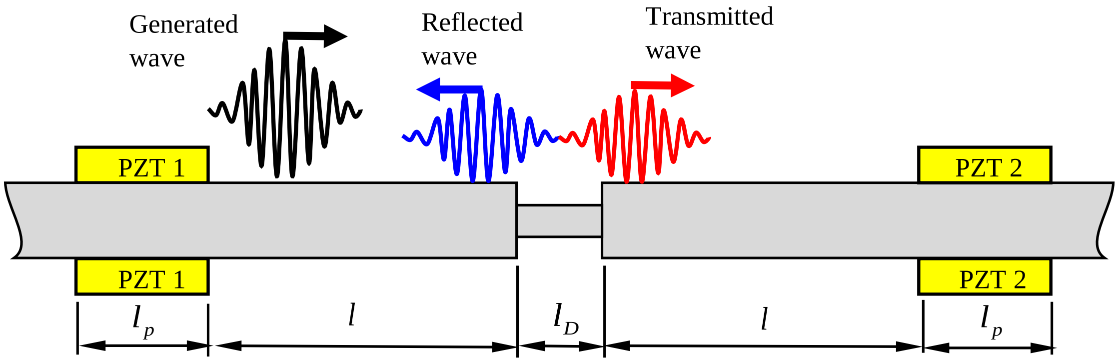

Source: Elaborated by the author.

4.3 Time Domain model

In the previous chapters frequency domain models were presented and analysed independently. In this chapter the complete model or system $H(\omega)$ is more complex and the analysis in the frequency domain is not necessarily the best. It is possible to analyse the behaviour of the propagation of elastic waves in the time domain. Such behaviour could be variation of amplitude, dispersion, the time taken for the wave packet to travel a certain distance, trend, quantity of energy reflected or transmitted, etc. (ZHONGQING; LIN, 2009).

There are two ways to obtain the response in time. The first, which is used in this dissertation, is by first formulating the model in the frequency domain, so that

$$V_{out}(\omega) = H(\omega)V_{in}(\omega), \tag{4.1}$$

where $V_{out}(\omega)$ and $V_{in}(\omega)$ are the voltage output from PZT 1 or PZT 2 and the voltage input to PZT 1 respectively as a function of frequency. The output voltage in the frequency domain is transformed to the time domain using the Inverse Fourier Transform. The second way, to obtain the output voltage in the time domain, is by

$$V_{out}(t) = h(t) * V_{in}(t), \tag{4.2}$$

where $*$ is the convolution operator and $h(t)$ is the Inverse Fourier Transform of the system $H(\omega)$ (KIHONG; HAMMOND, 2008).

4.4 Simulations

The input voltage is applied to the actuator is a wave packet consisting of a sine wave which has ten-cycles multiplied by a Hanning window.

To illustrate the way in which waves interact with the symmetric damage, a specific case is considered, where the parameters of the input data are shown in Table 3.

Table 3 - Data for processing of the signal.

Signal processing data		
Property	**value**	**units**
Frequency of excitation	100	kHz
time of the signal	$1x10^{-4}$	s
Sampling frequency	$3x10^{3}$	kHz
History time (Longitudinal wave)	$10x10^{-4}$	s
History time (Flexural wave)	$8x10^{-3}$	s

Source: Elaborated by the author.

This configuration, shown in Figure 24 is considered, in which the material properties of the elements are given in Table 1 and 2, and the geometric properties are given in Table 4.

Table 4 - Geometric properties of the beam and the piezoelectric of the system shown in Figure 23.

Geometric properties of the aluminium beam			
Property	**symbol**	**value**	**units**
Width	b	14	mm
Thickness	h	2	mm
Length	l	398	mm
Damage length (Longitudinal wave)	l_D	12.75	mm
Damage length (flexural wave)	l_D	1.36	mm
Geometric properties of the PZT elements			
Property	**symbol**	**value**	**units**
Width	b_p	14	mm
Thickness	h_p	0.19	mm
Length (Longitudinal wave)	l_p	25.5	mm
Length (flexural wave)	l_p	6.8	mm

Source: Elaborated by the author.

To illustrate the signals in the time and the frequency domains, Figures 24 and 25 show simulations of longitudinal waves in the system without and with damage (50% reduction in thickness of the beam) for pulse-echo and pitch-catch respectively. Figures 26 and 27 show corresponding simulations of flexural waves in the system without and with damage (50%) for pulse-echo and pitch catch respectively.

Each Figure shows an overview of the methodology used. It can be seen the input, the system and the output as important parts, in the centre of the diagram there is a box representing the system and the arrows going in and out, indicating ‘cause and effect’ relationship.

The input is shown in both the time and frequency domain on the left-hand side of the figures. The impulse response and the frequency response of the system are shown for the undamaged and damaged case. The voltage output from the PZT sensors are shown on the right-hand side of the figures in both time and frequency domains for the undamaged and damaged cases.

Figure 24 - Diagram of the system for the longitudinal waves in Pulse-echo configuration with the input, output and transfer function in time and frequency domain with 0% damage; solid blue line —, 50% damage; solid red line —.

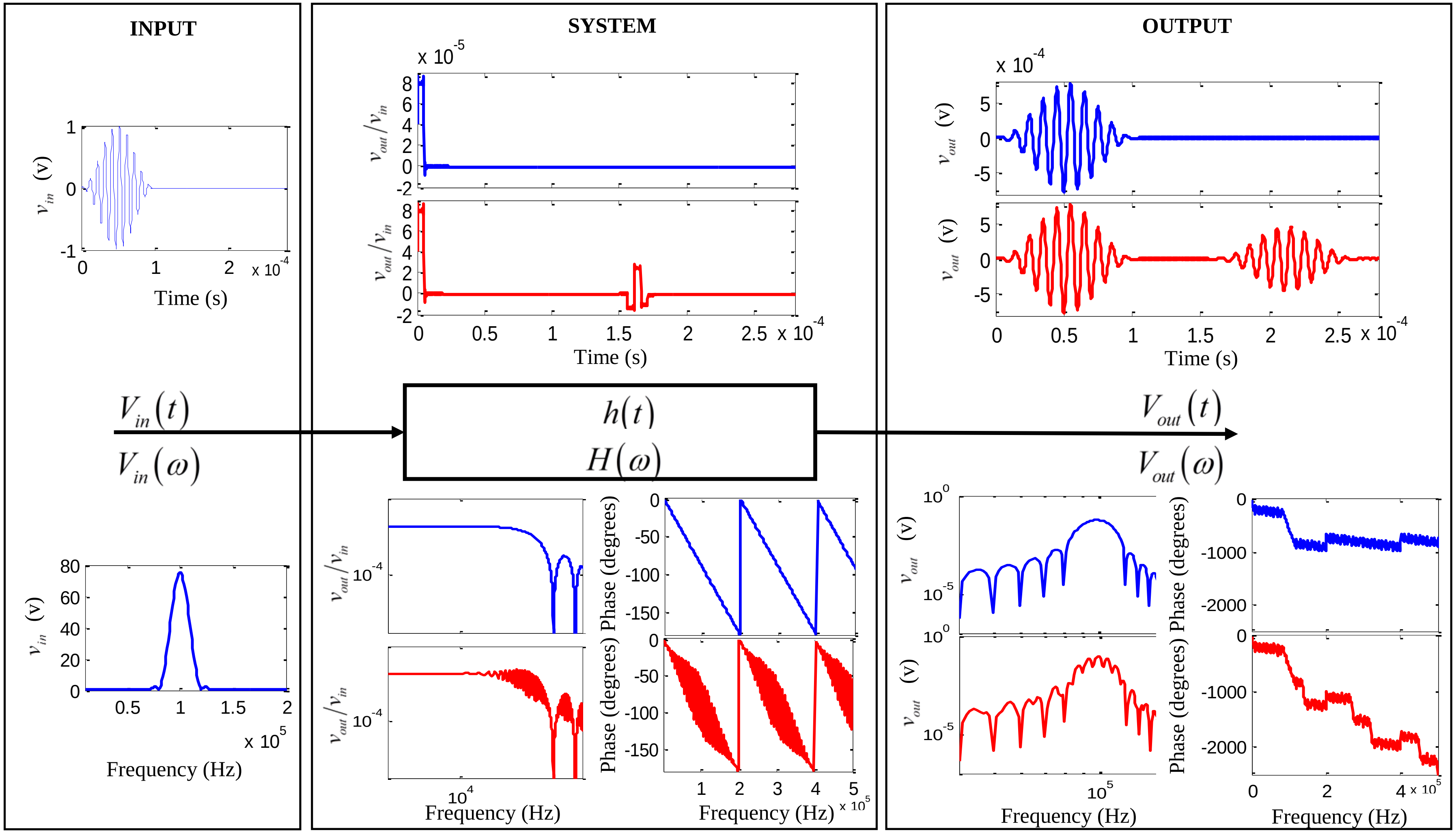

Source: Elaborated by the author.

Figure 25 - Diagram of the system for the longitudinal waves in Pitch catch configuration with the input, output and transfer function in time and frequency domain with 0% damage; solid blue line —, 50% damage; solid red line —.

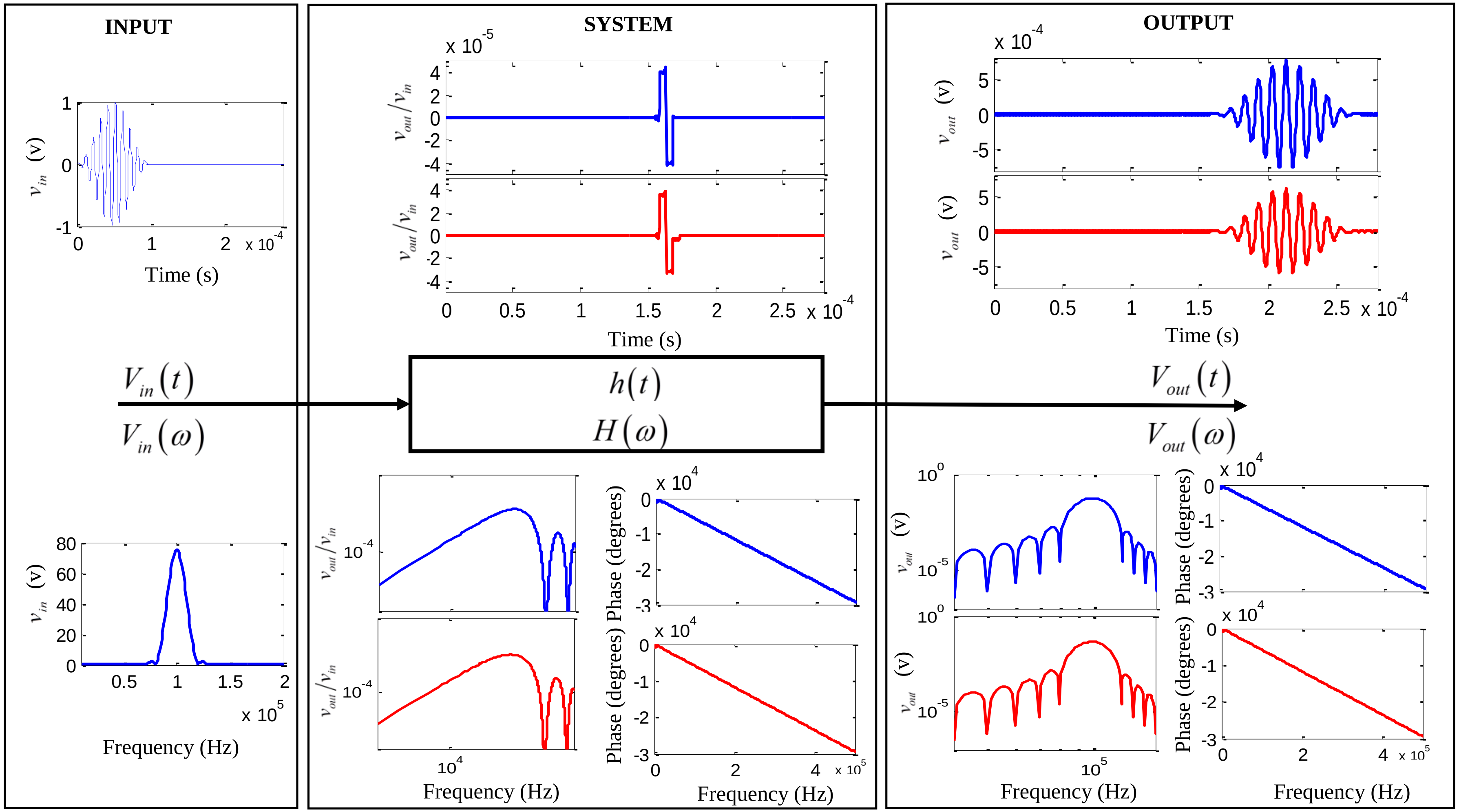

Source: Elaborated by the author.

Figure 26 - Diagram of the system for the flexural waves in Pulse-echo configuration with the input, output and transfer function in time and frequency domain with 0% damage; solid blue line —, 50% damage; solid red line —.

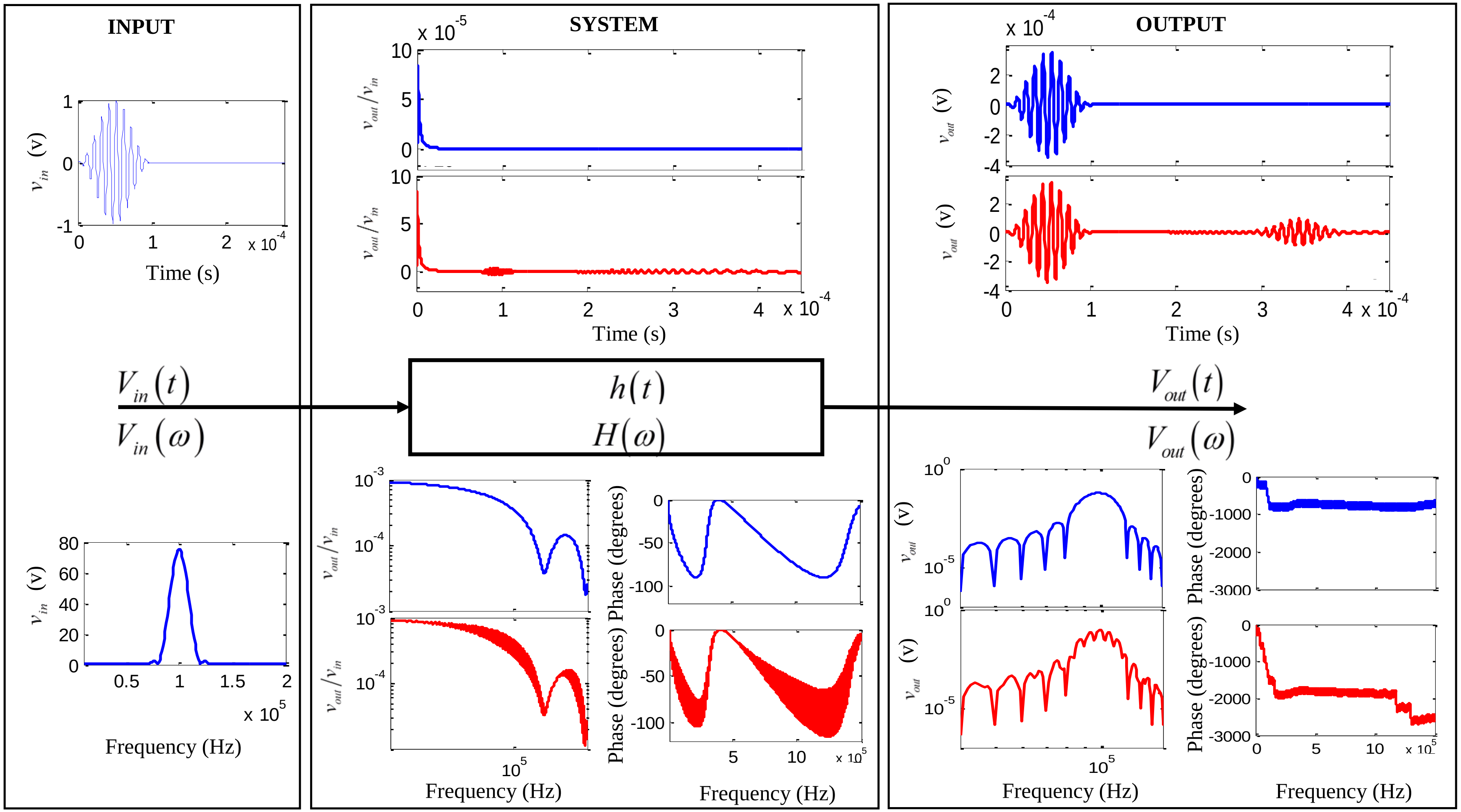

Source: Elaborated by the author.

Figure 27 - Diagram of the system for the flexural waves in Pitch catch configuration with the input, output and transfer function in time and frequency domain with 0% damage; solid blue line —, 50% damage; solid red line —.

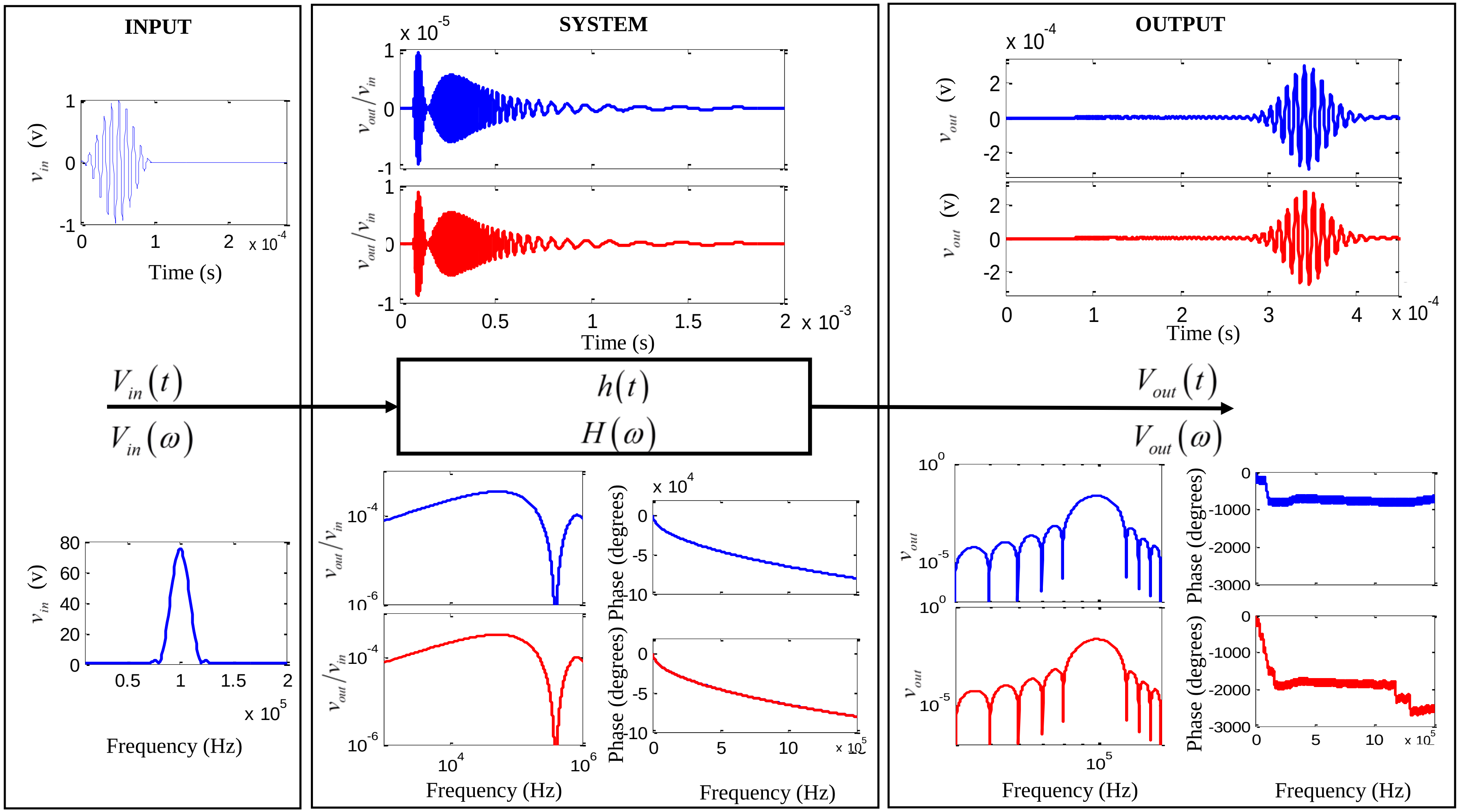

Source: Elaborated by the author.

4.4.1 Analysis of the system response with longitudinal waves

In this section, the time domain behaviour is studied, for a reduction in thickness of the beam of 0%, 10%, 30% and 50% of damage for pulse-echo and pitch-catch configurations.

The data in Table 4 were used to determine the ratios $l_D/\lambda_l = 1/4$ and $l_p/\lambda_l = 1/2$ which were used in the simulation. The simulations for longitudinal waves are shown in Figures 28a and b for the reflected wave and transmitted wave respectively.

It can be seen that the transmitted wave does not change dramatically as the damage increases, the peak changing by only about 20% when the damage is 50%. The reflected wave, however, is more sensitive, there is zero response when there is no damage, but the peak is about 60% of the incident wave when the damage is 50%.

Insets in Figure 28a and b is a close-up of the peak. It can be seen that there is no change in the phase of the wave packet as the damage increases.

Figure 28 - Simulation of (a) Pulse echo and (b) Pitch catch configuration due to an incident longitudinal wave with $l_D/\lambda_l = 1/4$ and $l_p/\lambda_l = 1/2$, for various percentages of symmetric damage; dashed dot magenta line −·−, 0% damage; dotted red line ..., 10% damage; dashed green line ---, 30% damage; thick solid blue line —, 50% damage.

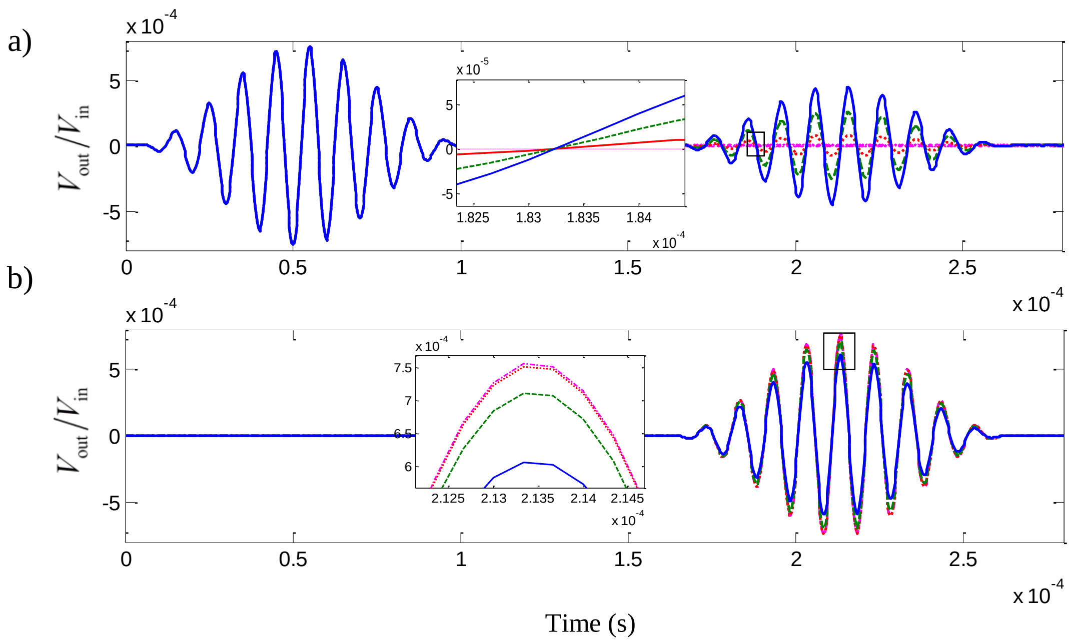

Source: Elaborated by the author

4.4.2 Analysis of the system response with flexural waves

In this section, as for the longitudinal wave, the time domain behaviour is studied for a reduction in thickness of the beam of 0%, 10%, 30% and 50% of damages for pulse-echo and pitch-catch configurations and they are shown in Figure 29a and b respectively.

The data in Table 4 were used to determine the ratios $l_D/\lambda_f = 1/10$ and $l_p/\lambda_f = 1/2$ which were used in the simulation. The simulations for flexural waves are shown in Figures 29a and b for the reflected wave and transmitted wave respectively.

As with the longitudinal wave, it can be seen that the transmitted wave does not change dramatically as the beam thickness is reduced. The peak changes by only about 6% when the damage is 50%. The reflected wave, however, is more sensitive, being 31% of the incident wave when the damage is 50%. The dispersion of the flexural wave can clearly be seen by comparing Figure 28a with Figure 29a. The insets in Figure 29a and b also show that there is some phase shift between the wave packets as the damage is increased. This is because of the changing wavespeed for varying thicknesses of beam as discussed above.

Figure 29 - Simulation of (a) Pulse echo and (b) Pitch catch configuration due to an incident flexural wave with $l_D/\lambda_f = 1/10$ and $l_p/\lambda_f = 1/2$, for various percentages of symmetric damage; dashed dot magenta line −·−, 0% damage; dotted red line ..., 10% damage; dashed green line ---, 30% damage; thick solid blue line —, 50% damage.

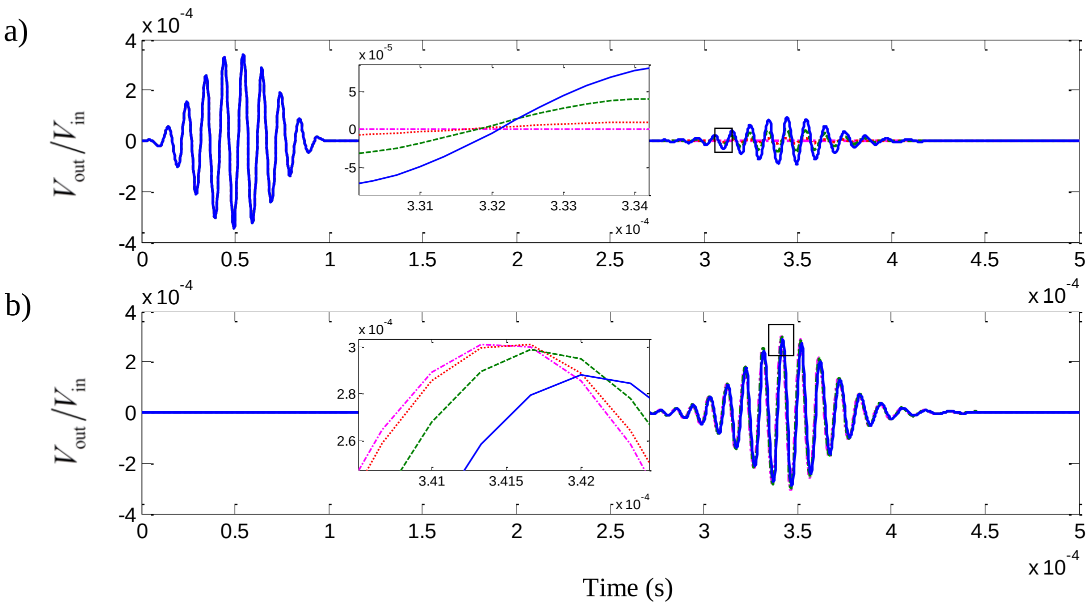

Source: Elaborated by the author

4.5 Discussion

The changes in the measured signals have a particular feature, is related to the damage. In this section, this relationship is studied for the pitch-catch and pulse-echo configuration. Here, a normalized damage index is used.

In the case of the pitch-catch configuration, the normalization is done dividing by the amplitude of the signal without damage. In the case of the pulse-echo configuration, the normalization is by dividing by the amplitude of the signal totally reflected, which results in a damage index of

$$\text{Damage Index} = \frac{\sum_{i=1}^{N} \sqrt{{y_i}^2}}{\sum_{i=1}^{N} \sqrt{{y_{b(i)}}^2}}, \tag{4.3}$$

where y_i is the i-th amplitude of the signal at the time t_i, $y_{b(i)}$ is the amplitude of the baseline case and N indicate the number of samples in each signal.

No energy is dissipated in the system so that the sum of the energy in the wave that reaches PZT 1 and the energy in the wave that reaches PZT 2 is equal to the energy in the wave launched by PZT 1. To check the conservation of energy between the incident, reflected and transmitted waves, a power index is also calculated.

$$\text{Power Index} = \frac{\sum_{i=1}^{N} {y_i}^2}{\sum_{i=1}^{N} {y_{b(i)}}^2}. \tag{4.4}$$

4.5.1 Damage index with longitudinal waves

Figure 30a shows plots of the reflected and transmitted longitudinal waves as a function of the percentage of damage. It can be seen that it is better to use the pulse-echo rather than pitch-catch configuration to detect the damage, especially in the range from 0-20% of damage. In this range, in the pulse-echo configuration, there is a one-to-one relationship between the reflected wave ratio and percentage damage. In the pitch-catch configuration, the transmitted wave for the same degree of damage is much less sensitive.

Figure 30b shows the normalised power in the reflected and transmitted waves as a function percentage of damages in solid blue line and dashed red line respectively. The sum of these is unity for all levels of damage (solid green line).

From the two Figures, it is possible to see that the curves intersect, when the amplitude ratio is 0.707 and the power amplitude ratio is 0.5 when the percentage of damage is about 60%. It means that for this level of damage, the reflected power is equal to the transmitted power.

Figure 30 - Relationship between the scattered longitudinal waves and damage with $l_D/\lambda_l = 1/4$ and $l_p/\lambda_l = 1/2$, (a) Damage index for reflected longitudinal waves, solid blue line — and transmitted longitudinal waves, dashed red line ---, (b) Power index for reflected longitudinal waves, solid blue line —, transmitted longitudinal waves, dashed red line --- and total power, dotted green line ····.

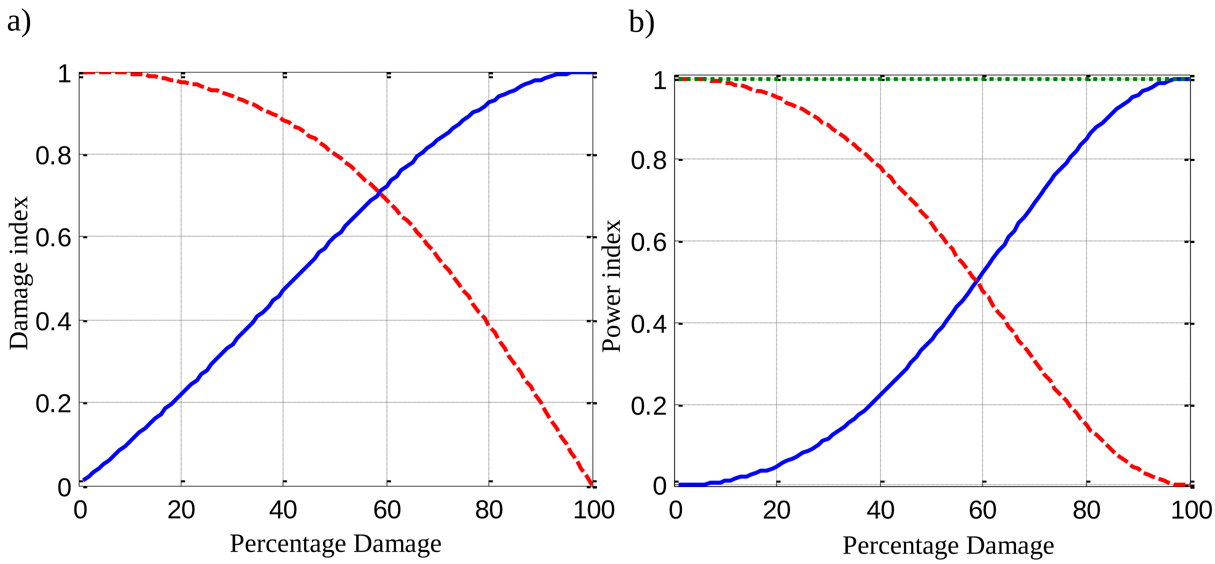

Source: Elaborated by the author.

4.5.2 Damage index with flexural waves

Figure 31a shows the responses of the reflected and transmitted flexural waves as a function of the percentage of damage. It can be seen that it is better to use to pulse-echo rather than pitch-catch to detect the damage, especially in the range from 0-60% of damage. In this range, for pulse-echo configuration, the damage is roughly proportional to the amplitude of the reflected wave.

It can be seen that above to 60% it begins to decrease before increasing again. This is because of the dispersive nature of the wave, which results in the behaviour shown in Figure 8.

For some situations a given frequency, l_D/λ_f , the reflected wave can decrease as the thickness is reduced. Note in Figure 8 that as the thickness reduces, the frequency at which there is no reflection decreases, but this is not the case for the longitudinal wave.

This fact is extremely important in the context of SHM, where normally an increase in the reflected wave means an increase in damage. As these results show, with a longitudinal wave this is the case, but for a flexural wave, then an increase in damage could result in a decrease in the reflected wave in some situations.

It is observed that there is a numerical error at a point close to 100% due to poor conditioning of the matrices for this condition.

As with longitudinal case, Figure 31b shows the normalised power in the reflected and transmitted waves as a function percentage of damage in solid blue line and dashed red line respectively. The sum of these is unity for all levels of damage (solid green line).

From the two Figures, it is possible to see, the same behaviour of the longitudinal analysis, the curves intersect, when the amplitude ratio is 0.707 and the power amplitude ratio is 0.5 when the percentage of damage is 60%. It means that for this level of damage, the reflected power is equal to the transmitted power.

Figure 31 - Relationship between the scattered flexural waves and damage with $l_D/\lambda_f = 1/10$ and $l_p/\lambda_f = 1/2$, (a) Damage index for reflected flexural waves, solid blue line — and transmitted flexural waves, dashed red line ---,. (b) Power index for reflected flexural waves, solid blue line —, transmitted flexural waves, dashed red line --- and total power, thick dotted green line ····.

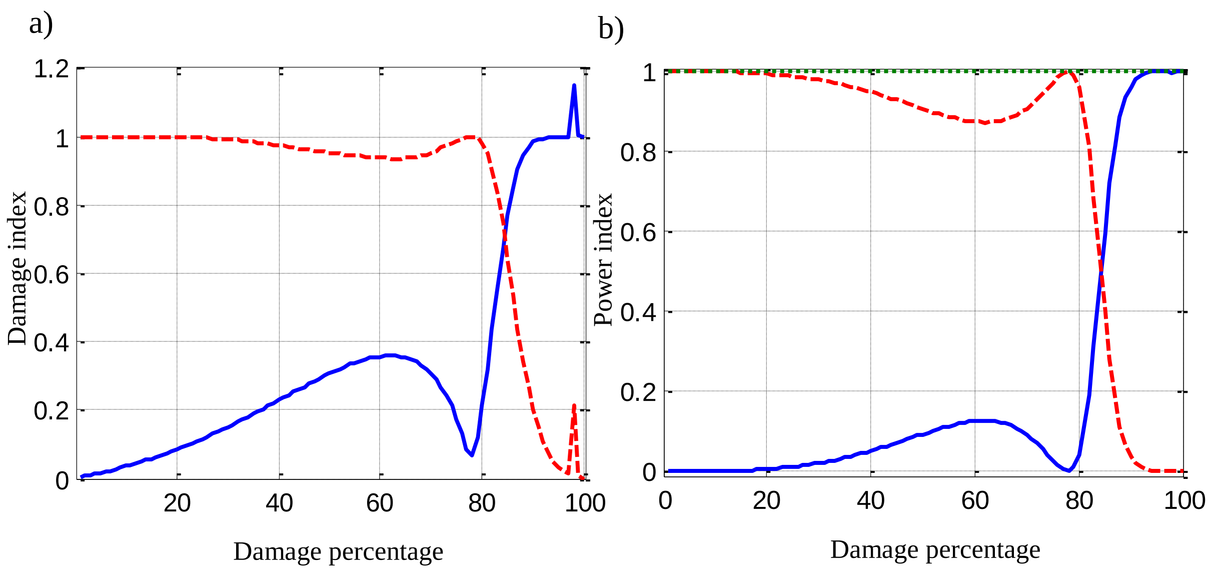

Source: Elaborated by the author.

4.5.3 Comparison between the effects of longitudinal and flexural waves for the same length of damage

In this section, simulations are presented, for two different lengths of damage (15 and 20mm). The configuration for this example is shown in Figure 32 in which the material properties of the elements are given in Table 1 and 2. The lengths of the actuator and sensors was chosen to be 10mm. Having set the length of damage, actuators and sensors to be fixed, frequencies of 50, 60 and 100 kHz were chosen as the frequencies of excitation. The time duration of each signal is shown in Table 5.

Figure 32 - Diagram of an aluminium beam with length damage l_D coupled with PZT elements

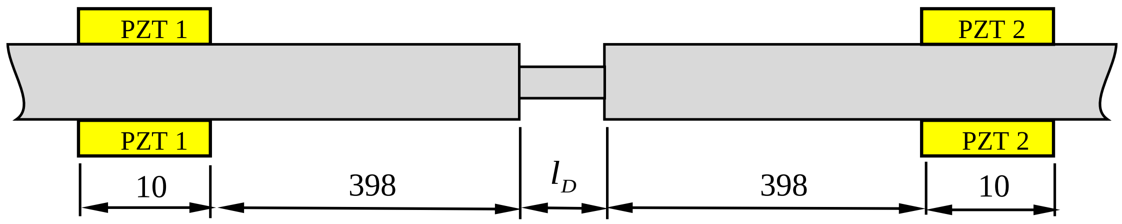

Source: Elaborated by the author.

Table 5 - Signal time for the frequency of excitation chosen for this simulation

Signal processing data	
Frequency of excitation (kHz)	**duration of the input signal (s)**
50	$2x10^{-4}$
60	$1.7x10^{-4}$
100	$1x10^{-4}$

Source: Elaborated by the author.

Table 6 shows the lengths of damage and PZT, wavelength for 50, 60 and 100 kHz, and their ratios calculated. With this table, it is possible to compare and check with the optimum values obtained in chapter 2 and 3. It can be seen that there are some ratios close to the optimum one in some cases, and other cases, they are not. This will have an impact on the plots for the damage index.

In Figure 33, the damage index as a function of the percentage damage is shown. Using longitudinal waves for 15mm of damage with 100 kHz as the frequency of excitation is a good choice as can be seen. For 20mm of damage with 60 kHz as the frequency of excitation can be seen a good response for detection of this length of damage. Using flexural waves for 15 and 20mm of damage with 100 kHz and 50 kHz respectively, there is a good response.

It can be seen for all the cases selected that the longitudinal waves are more sensitive than the flexural waves for identification of symmetric damage, and it can be seen that pulse-echo configuration is more sensitive than pitch-catch configuration.

Table 6 - Length of damage, length of PZT, wavelength for 50, 60 and 100 kHz and their ratios calculated.

Parameter	**unit.**	**Optimum**	**50khz**		**60khz**		**100khz**	
l_D	mm		**15**	**20**	**15**	**20**	**15**	**20**
λ_l	mm		102	102	85	85	51	51
λ_f	mm		19.2	19.2	17.6	17.6	13.6	13.6
l_p	mm		10	10	10	10	10	10
l_D/λ_l	[-]	**0.25**	0.15	0.20	0.18	0.24	0.29	0.39
l_D/λ_f	[-]		0.78	1.04	0.85	1.14	1.10	1.47
l_p/λ_l	[-]	**0.5**	0.10	0.10	0.12	0.12	0.20	0.20
l_p/λ_f	[-]	**0.5**	0.52	0.52	0.57	0.57	0.74	0.74

Source: Elaborated by the author.

Figure 33 - Damage index as a function of percentage damage for the example in Figure 32. Using frequencies of excitation: (a) 50 kHz, (b) 60 kHz and (c) 100 kHz. It is shown the reflected and transmitted longitudinal waves, in solid blue line —; and dashed red line --- respectively; and the transmitted and the reflected flexural waves, in dotted black line ····; and dashed dot green line -·- respectively.

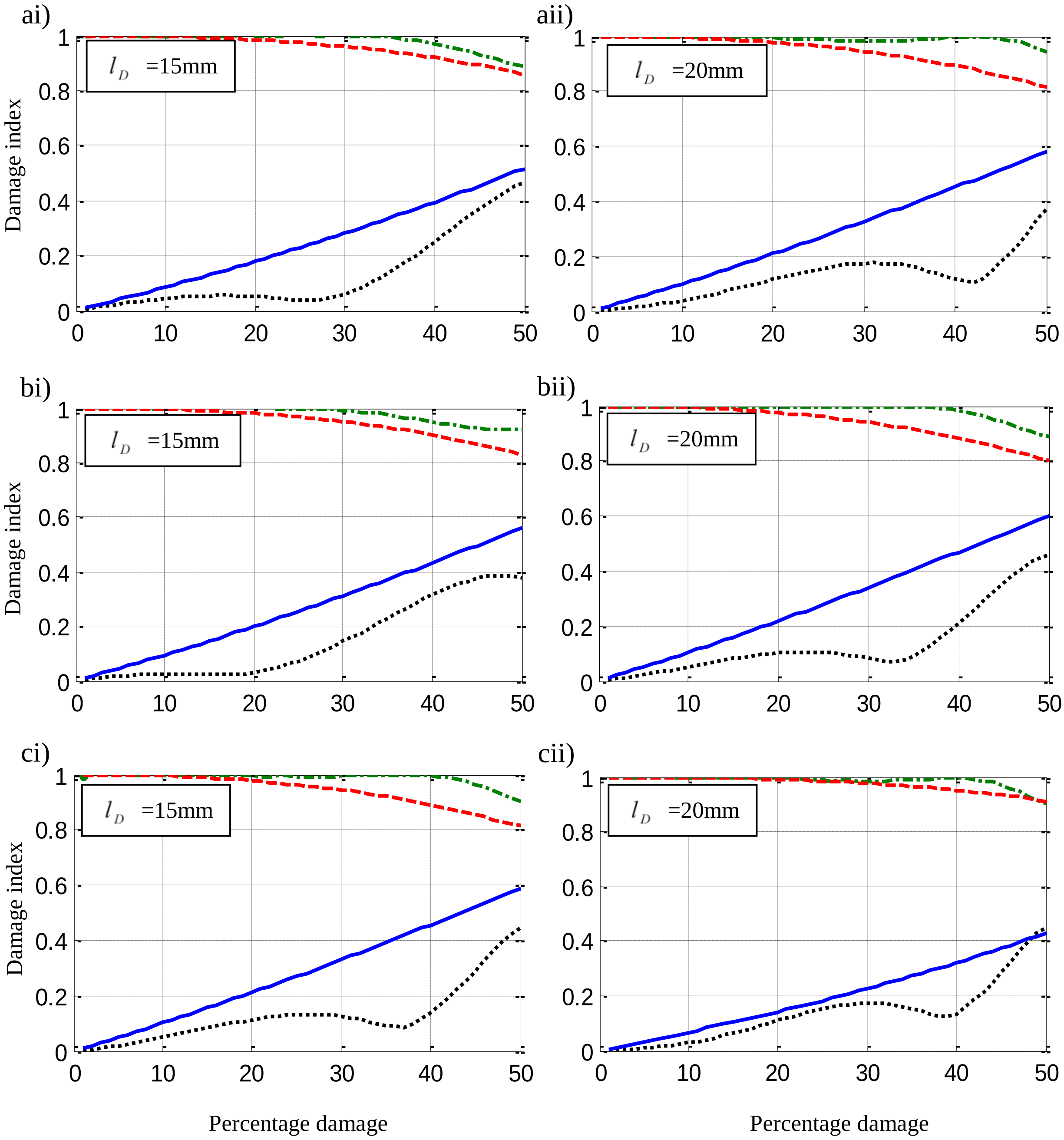

Source: Elaborated by the author.

4.6 Conclusions

In this chapter, the complete system has been presented: beam, PZT elements and symmetric damage section for longitudinal and flexural waves. It was configured in pulse echo and pitch-catch and was investigated in the time domain.

Two kind of examples were discussed using the Damage index. The first one, with optimal parameters of ratio l_D/λ and l_p/λ, was excited with optimum frequencies to obtain the best response that the system can give to identify a damage. In the second one, the size of the piezoelectric elements and the size of damage were fixed (found more in practice). The best excitation frequency for these conditions was selected. As a result, it was found that it is better to measure reflected than transmitted waves as the change in these wave amplitudes, this is more pronounced for small increases of percentage damage in a section of the beam.

It was also found that the longitudinal waves are more sensitive than flexural waves, to symmetric damage in a section of the beam.

5 CONCLUSIONS

5.1 Summary of the Dissertation

This Chapter summarizes the work done in this dissertation and presents the main conclusions obtained as well as the recommendations for further work. The principal objectives in this dissertation were to develop a wave propagation model of a one-dimensional structure with symmetric damage coupled with PZT actuator and sensor in two configurations to sense reflected and transmitted waves and to analyse the effects of the size of piezoelectric and symmetric damage both in frequency and time domain. To achieve these objectives the dissertation was organized as follows:

In Chapter 1 the general idea for this dissertation was presented. The fundamentals of Structural Health Monitoring (SHM) and the application of wave propagation in SHM was discussed, and a review of the literature was carried out.

In Chapter 2 the theory of wave propagation was presented using longitudinal waves in bars and flexural wave in beams. The phenomenon of dispersion of flexural waves was described as well as the group velocity. A wave model was then developed to investigate the effect of longitudinal and flexural waves on damage section of the beam. The simulations presented in this chapter gave clear information about the behaviour of the reflected and transmitted waves due to their interaction with a damaged section of the beam that was symmetric with respect to the neutral axis of the beam.

In Chapter 3 models of a piezoelectric actuator and sensor were presented. The way in which they generate and sense longitudinal and flexural wave was investigated, obtaining important parameters. Simulations were carried out, showing the behaviour of the actuator and sensor.

In Chapter 4 a complete system consisting of actuator, damage and sensors was studied. The system modelled in frequency domain, which was then transformed into the time domain using the inverse Fourier Transform. In the time domain, the complete system with the optimal parameters (determined in chapters 2 and 3) was simulated to determine the reflected and transmitted longitudinal and flexural waves for the damaged section of the beam. Finally, the relationship between the reflected and transmitted waves and the damage was studied by way of a Damage index.

5.2 Main Conclusions

The main conclusions from this dissertation are as follows:

- Longitudinal waves have a different behaviour with respect to flexural waves when they interact with damage that is symmetric with respect to the neutral axis of the beam. In the longitudinal case, the greater the reduction in beam thickness in the damaged section of beam, the greater the amplitude of the reflected waves. In the flexural case, depending of the parameter selected, the reflected wave amplitude increases and in some situations, it is possible for the reflected waves amplitudes to decrease rather than increase as the beam thickness is reduced.
- With respect to the behaviour of the response of the piezoelectric element with longitudinal and flexural waves, it was found that optimum responses are obtained when the length of the PZT element is a half a wavelength. Waves are strongly excited and sensed. In this condition if the length of the PZT element is equal to one wavelength, the waves cannot be excited or sensed.
- With longitudinal waves in the complete system (beam with symmetric discontinuity and piezoelectric elements) is possible to show that the PZT element will detect damage equal to half of length of the PZT with optimal response.
- Longitudinal waves are more sensitives than flexural waves, for identifying symmetric damage in a section of the beam.
- In general, for high frequencies waves (longitudinal and flexural waves), it is better to measure with reflected waves rather than transmitted waves as the change in these wave amplitudes, this is more pronounced for small damages in section of the beam.

5.3 Recommendation for Further Work

The use of high frequency waves, for detecting damages in structural waveguides, studied in this dissertation, is a basis for the comprehension and development of further works as described below

- In this dissertation, an Euler Bernoulli beam with a symmetric damage was analysed using piezoelectric elements. The next step for a further work could be the theoretical analysis of the same system with an asymmetric damage.
- Experimental verification of the result in this dissertation.
- Theoretical and experimental works could be developed applying high order waveguides, for example Timoshenko theory applied in beams, the higher-order theories provide more accurate description of the motion at high frequencies than elementary theories (LEE, 2006).
- The study could be extended to two or three-dimensional structures where the element is reducible to one-dimension for example a thin uniform rectangular plates.
- Localization of damage for one-dimensional guided structures could be studied using the properties of group velocity.
- The research could be extended to study the sensitivity of the impulse or frequency response to damage.

REFERENCES

ADAMS, D. E. **Health monitoring of structural materials and components**. West Sussex: John Wiley & Sons, 2007. 460 p.

BRENNAN, M. J. **Active control of waves on one-dimensional structures**. 1994. 342f. Thesis (PhD in Mechanical Engineering) - Faculty of Engineering and Applied Science, Institute of Sound and Vibration Research, Southampton, 1994.

CAWLEY, P.; ALLEYNE, D. **Practical long range guided wave inspection–managing complexity**. Disponível em: < http://www.ndt.net/article/mendt03/4/4.htm>. Acesso em: 15 mar. 2015.

CRAWLEY, E. F.; ANDERSON, E. H. Detailed models of piezoceramic actuation of beams. **Journal of Intelligent Material Systems and Structures**, Lancaster, v. 1, p. 4-25, 1990.

DOEBLING, S. W.; FARRAR, C. R.; PRIME, M. B. A.; HEVITZ, D.W. **Damage identification and health monitoring of structural and mechanical systems from changes in their vibration characteristics: a literature review**. Los Alamos: National Laboratory, USA, 1996. 134 p. Disponível em: <https://institute.lanl.gov/ei/shm/pubs/lit_review.pdf>. Acesso em: 15 oct. 2013.

DOEBLING, S. W.; FARRAR, C. R.; PRIME, M. B. A. **Summary review of vibration-based damage identification methods.** Los Alamos: National Laboratory, 1998. Disponível em: <http://public.lanl.gov/prime/doebling_svd.pdf>. Acesso em: 15 oct. 2013.

DOYLE, J. F. **Guided explorations of the mechanics of solids and structures**. New York: Cambridge University, 2009. 447 p.

FAHY, F.; GARDONIO, P. **Sound and structural vibration**. 2. ed. Rio de Janeiro: Elsevier, 2007. 656 p.

FARRAR, C. R.; WORDEN K. **Structural health monitoring**: a machine learning perspective. New York: John Wiley & Sons 2013. 654 p.

GIURGIUTIU, V. **Structural health monitoring with piezoelectric wafer active sensors**. New York: Elsevier, 2008. 760 p.

GRAFF, K. F. **Wave motion in elastic solids**. Oxford: Clarendon 1975. 649 p.

INMAN, D. J. Smart structures: examples and new problems. In: CONGRESSO BRASILEIRO DE ENGENHARIA MECÂNICA – COBEM, 16, 2001, Uberlândia. **Anais...** Uberlândia: ABCM. 2001. p. 26-30.

KIHONG, S.; HAMMOND, J. K. **Fundamentals of signal processing**. New York: John Wiley & Sons 2008.

LARICO, R. F.; LOPES, P. H.; MANZONI, A. F.; DE ARAGAO, B. J. G.; SILVA, E. S.; SANTOS, T. F. A.; ASSIS, V. A. Improvements in post-processing of signals acquired from a lamb wave based SHM system for detecting corrosion in aluminium. In: EUROPEAN-AMERICAN WORKSHOP ON RELIABILITY OF NDE, 5, Berlin. **Proceedings of the…** Berlin: [s.n.], 2013. (Poster, 25).

LEE, B. C.; STASZEWSKI, W. J. Modelling of Lamb waves for damage detection in metallic structures: Part I. Wave propagation. **Journal of Smart Material and Structure**, Bristol, v. 12, p. 804-814, 2003.

LEE, S. **Wave reflection, transmission and propagation in structural waveguides**. 2006. 267 f. Thesis (PhD in Mechanical Engineering) - University of Southampton, Southampton, 2006.

MICHAELS, T. E.; RUZZENEB, M.; MICHAELS, J. E. Frequency-wavenumber domain methods for analysis of incident and scattered guided wave fields. In: KUNDU, T. (Ed.). **Health Monitoring of Structural and Biological Systems, Proceeding of SPIE**, v. 7295, 2009. 12 p.

MACE, B. R. Wave reflection and transmission in beams. **Journal of Sound and Vibration**, London, v. 97, n. 2, p. 237-246, 1984.

OSTACHOWICZ, W.; KUDELA, P.; KRAWCZUK, M.; ZAK, A. **Guided waves in structures for SHM**: the time-domain spectral element method. West Sussex: John Wiley & Sons, 2012.

RAGHAVAN, A.; CESNIK, C. E. S. Modelling of piezoelectric-based Lamb-wave generation and sensing for structural health monitoring. LIU, S.-C. **Smart Structures and Materials 2004:** sensors and smart structures technologies for civil, mechanical, and aerospace systems. Bellingham: [s.n], 2004. (Proc. of SPIE Vol. 5391)

ROUSSEAU, M.; MACE, B. R.; WATERS T. P. An audio-frequency wave technique for damage detection in beams. **Key Engineering Materials**, Switzerland, v. 245/246, p. 433-442, 2003.

RYUE, J.; THOMPSON, D. J.; WHITE, P. R.; THOMPSON, D. R. Wave reflection and transmission due to defects in infinite structural waveguides at high frequencies. **Journal of Sound and Vibration**, London, v. 330 p. 1737–1753, 2011.

SHONE, S. **A flexural wave scattering method for damage detection in beams**. 2006. 230 f. Thesis (PhD in Mechanical Engineering) - University of Southampton, Southampton, 2006.

STEPIMSKI, T.; UHL, T.; STASZEWSKI, W. **Advanced structural damage detection**: from theory to engineering applications. Bristol: John Wiley & Sons, 2013. 352 p.

TENENBAUM, R. A.; STUTZ, L. T.; FERNANDES, K. M. Comparison of vibration and wave propagation approaches applied to assess damage influence on the behaviour of Euler–Bernoulli beams. **Journal of Computers and Structures**, Elmsford, v. 89, p. 1820–1828, 2011.

VASQUES, C. H. **Efeitos de descontinuidades na propagação de ondas em estruturas unidimensionais**. 2013. 116 f. Dissertação (Mestrado em Engenharia Mecânica) – Faculdade de Engenharia, Universidade Estadual Paulista, Ilha Solteira, 2013.

WANG, B.; ROGERS, C. A. Modeling of finite-length spatially-distributed induced strain actuators for laminate beams and plates. **Journal of Intelligent Material Systems and Structures**, Lancaster, v. 2, p. 38-58, 1991.

WANG, X.; TSE, P. W.; MECHEFSKE C. K.; HUA, M. Experimental investigation of reflection in guided wave-based inspection for the characterization of pipeline defects. **NDT & E International**, London, v. 43, p. 365-374, 2010.

ZHONGQING, S. U.; LIN, Y. E. Identification of damage using lamb waves: from fundamentals to applications. **Lectures Notes in Applied and Computational Mechanics.** Berlin: Springer-Verlag, 2009. v. 48.

APPENDIX A

1. Matlab code for complete system beam-PZT-damage with longitudinal waves

```
%%
% Simulation using longitudinal waves of the complete Model with actuator,
% sensor and symmetric damage
% Results
% -Input Voltage in frequency and time domain
% -interaction of the wave with damage
% -IRF and FRF
% -Output Voltage in frequency and time domain
% -Damage Index and Power index
clear all;clc;close all;
%% properties of the beam
E=71e9;                    % Young's modulus (N/m2)
rho=2730;                  % Density (kg/m3)
b=14e-3;                   % width (m)
h=2e-3;                    % thickness (m)
I=b*h^3/12;                % Second moment of area (m3)
A=b*h;                     % Cross-sectional area (m2)
L1=0.3975;                 % Length before the damage (m)
L2=0.3975;                 % Length after the damage (m)
EI=E*I;                    % Flexural rigidity
EA=E*A;                    % In-plane stiffness
%% properties of the PZT-PSI-5A4E PZT from Piezo Systems, INC.
Ea=6.6e10;                 % Young's modulus (N/m2)
ha=1.91e-4;                % thickness(m)
ba=14e-3;                  % width(m)
d31=-190e-12;              % material strain constant (m/v)
la=0.0255;                 % length of actuator 0.0255
l1=0.0255;                 % length of sensor 1
l2=0.0255;                 % length of sensor 2
c=430e-9;                  % Capacitance of the sensor (F)
%% parameters of signal processing
fs=3000000;                % Sampling Frequency (Hz)
dt=1/fs;                   % Resolution (s)
tf=10e-4;                  % time (s)
df=1/tf;                   % Resolution (Hz)
f=0:df:fs/2;               % vector frequency
t=0:dt:tf;                 % vector time
%% parameters of voltage input
freq = 100000;             % frequency of the signal (Hz)
Vin=1;                     % voltage Amplitude
tf1=1e-4;                  % time of the signal (s)
dt1=1/fs;                  % Resolution (s)
t1=0:dt1:tf1;              % vector time of signal (s)
%% voltage input
ftt=zeros(size(t));
ft1=Vin*sin(2*pi*freq*t1);
fh=hann(length(ft1));
fw=fh.*ft1';
ftt(1:length(t1))=fw;
ft=ftt;
FT=fft(ft);
%% Plotting voltage input
% INPUT VOLTAGE TIME DOMAIN
figure (1)
plot(t,ft)
```

```
title('INPUT VOLTAGE ON TIME DOMAIN')
xlabel('time (s)')
ylabel('Voltage (V)')

% INPUT VOLTAGE FREQ DOMAIN
figure (2)
semilogx(f,abs(FT(1:length(f))))
title('INPUT VOLTAGE ON FREQ DOMAIN')
xlabel('freq (Hz)')
ylabel('Voltage (V)')
%% Preallocating Arrays
r=zeros(1,length(f));
s=zeros(1,length(f));
oa2v=zeros(1,length(f));
oa3v=zeros(1,length(f));
lambda=zeros(1,length(f));
lambda1=zeros(1,length(f));
oa2v_A=zeros(1,length(f));
oa3v_A=zeros(1,length(f));
oa2v_a=zeros(100,length(f));
oa3v_a=zeros(100,length(f));
vout2l=zeros(1,length(f));
vout1l=zeros(1,length(f));
vout3l=zeros(1,length(f));
vout1l_v=zeros(100,length(f));
vout2l_v=zeros(100,length(f));
vout1l_vt=zeros(100,length(t));
vout2l_vt=zeros(100,length(t));
V2_v=zeros(100,length(f));
v2_v=zeros(100,length(t));
V1_v=zeros(100,length(f));
v1_v=zeros(100,length(t));
lambdad=zeros(1,length(f));
rld=zeros(1,length(f));
%%
px1_s1=zeros(100,1);
py1_s2=zeros(100,1);
px2_s1=zeros(100,1);
py2_s2=zeros(100,1);
%% calculating the response
Dam=0:1:100;
for j=1:101
n=0;

for fq=0:df:fs/2;                  % Frequency
n=n+1;
w=2*pi*fq;                         % circular frequency
kb=(rho*A/(EI))^.25*w.^.5;         % flexural wavenumber
lambda(n)=2*pi/kb;
% rl(n)=la*(rho/E)^.5*fq;          % Ratio length actuator to long. wavelength
kl=(rho/E)^.5*w;                   % Longitudinal wavenumber
lambda1(n)=2*pi/kl;                % Flexural wavenumber

HB=[0 0 1 0 0 1;
   1 1 0 1 1 0;
   kb 1i*kb 0 -kb -1i*kb 0;
   EI*kb.^2 -EI*kb.^2 0 EI*kb.^2 -EI*kb.^2 0;
   EI*kb.^3 -1i*EI*kb.^3 0 -EI*kb.^3 1i*EI*kb.^3 0;
   0 0 1i*EA*kl 0 0 -1i*EA*kl];
%% state vector-wave matrix of damaged section
```

```
% properties of the damaged section of beam

Ld=12.75/1000;                    % Length of the damaged section (mm)
Ed=71e9;                          % Young's modulus (N/m2)
rhod=2730;                        % Density (kg/m3)
td=1-Dam(j)/100;
bd=14e-3;hd=2e-3*td;              % width and thickness (m)
Ad=bd*hd;                         % Cross-sectional area
Id=bd*hd^3/12;                    % Second moment of area
EId=Ed*Id;                        % Flexural rigidity
EAd=Ed*Ad;                        % In-plane stiffness
kbd=(rhod*Ad/(EId))^.25*w.^.5;  % flexural wavenumber
kld=(rhod/Ed)^.5*w;               % Longitudinal wavenumber
lambdad(n)=2*pi/kbd;
lambdad(n)=2*pi/kbd;
rld(n)=Ld*(rhod/Ed)^.5*fq;        % Ratio length damage to long. wavelength

HD=[0 0 1 0 0 1;
   1 1 0 1 1 0;
   kbd 1i*kbd 0 -kbd -1i*kbd 0;
   EId*kbd.^2 -EId*kbd.^2 0 EId*kbd.^2 -EId*kbd.^2 0;
   EId*kbd.^3 -1i*EId*kbd.^3 0 -EId*kbd.^3 1i*EId*kbd.^3 0;
   0 0 1i*EAd*kld 0 0 -1i*EAd*kld];

%% wave transmission ratio defect
TD=[exp(kbd*Ld) 0 0 0 0 0;
   0 exp(1i*kbd*Ld) 0 0 0 0;
   0 0 exp(1i*2*pi*rld(n)) 0 0 0;
   0 0 0 exp(-kbd*Ld) 0 0;
   0 0 0 0 exp(-1i*kbd*Ld) 0;
   0 0 0 0 0 exp(-1i*2*pi*rld(n))];
%% wave transmission ratio L1 side
TL1=[exp(kb*L1) 0 0 0 0 0;
   0 exp(1i*kb*L1) 0 0 0 0;
   0 0 exp(1i*kl*L1) 0 0 0;
   0 0 0 exp(-kb*L1) 0 0;
   0 0 0 0 exp(-1i*kb*L1) 0;
   0 0 0 0 0 exp(-1i*kl*L1)];
%% wave transmission ratio L2 side
TL2=[exp(kb*L2) 0 0 0 0 0;
   0 exp(1i*kb*L2) 0 0 0 0;
   0 0 exp(1i*kl*L2) 0 0 0;
   0 0 0 exp(-kb*L2) 0 0;
   0 0 0 0 exp(-1i*kb*L2) 0;
   0 0 0 0 0 exp(-1i*kl*L2)];
%% wave transmission ratio L1 side
L3=L1+la-l1;
TL3=[exp(kb*-L3) 0 0 0 0 0;
   0 exp(1i*kb*-L3) 0 0 0 0;
   0 0 exp(1i*kl*-L3) 0 0 0;
   0 0 0 exp(-kb*-L3) 0 0;
   0 0 0 0 exp(-1i*kb*-L3) 0;
   0 0 0 0 0 exp(-1i*kl*-L3)];
%% wave_actuator_single - Equation for one side
tt=E*b*h/(Ea*ba*ha);
DD=d31*Vin/ha;
F=2*h*E*b*DD/(6+tt); % strain energy model
% Longitudinal Amplitude generated by the initial wave propagation of PZT
al0=(1i*F/(2*E*A*(kl)))*(1-exp(1i*kl*(la)));
al0_e=al0*exp(-1i*kl*(la));
```

```
%% Analyzing before the sensor 2 for normalization (quantification)
L=L1+L2;                        % Position before the sensor 2
al0_ex=al0_e*exp(-1i*kl*(L));
%% Calculate matrices relating the incoming and outgoing waves
ai=[0;0;0;0;0;al0_e];           % Wave Amplitude vector initial from actuator 1
a1=TL1*ai;
HH = HD*TD*(HD\HB);
B=[HB(:,1:3) HH(:,4:6)];
C=[HH(:,1:3) HB(:,4:6)];
 oa1=C\B*a1;

s(n+1)=oa1(6);
if isnan(s(n+1));
s(n+1)=s(n);
end
vv=[0;0;0;0;0;s(n+1)];

r(n+1)=oa1(3);
if isnan(r(n+1));
r(n+1)=r(n);
end
v=[0;0;r(n+1);0;0;0];

%% % going to sensor 2
oa2=TL2*vv;
oa2_right=oa2(6);
oa2v=oa2_right;
oa2v_A(n)=oa2v./al0_e;
oa2v_A(1)=0;
%% % going to sensor 1
oa3=TL3*v;
oa3_left=oa3(3);
oa3v=oa3_left;
oa3v_A(n)=oa3v./al0_e;
oa3v_A(1)=0;
%% Calculate the output voltage in the sensor-2
% Longitudinal difference in the sensor 2
dif_lo2= oa2(6)*(1-exp(-1i*kl*l2));
% Carge generated by longitudinal wave
q_long_2=d31*Ea*ba*dif_lo2;
% Voltage generated in the sensor 2 by Longitudinal waves
vout_2l=q_long_2/c;
% Voltage generated in the sensor 2 by Longitudinal waves for all freq.
vout2l(n)=vout_2l;
vout2l(1)=0;
%% Calculate the output voltage in sensor-1
% Longitudinal difference from the defect to the sensor 1
dif_lo1= oa3(3)*(1-exp(-1i*kl*l1));
% Longitudinal difference from the actuator to the sensor 1. (Turn off for quantification, plots 16-17)
dif_lo11=0;%(1i*F/(EA*kl))*(exp(-1i*kl*l1)-1);
% Longitudinal total difference
dif_tot_l=dif_lo1+dif_lo11;
% Carge generated by longitudinal waves
q_long_1=d31*Ea*ba*dif_tot_l;
% Voltage generated in the sensor 1 by Longitudinal waves
vout_1l=q_long_1/c;
% Voltage generated in the sensor 1 by Longitudinal waves for all freq.
vout1l(n)=vout_1l;
vout1l(1)=0;
%% Calculate the output voltage in sensor-3 for quantification sensor 1(this is only to normalize the sensor 1)
```

```
% Longitudinal difference of reflected waves from the damage to sensor 1
dif_lo3= al0_ex*(1-exp(-1i*kl*l1));
qtotal_3=d31*Ea*ba*dif_lo3;
vout3l(n)=qtotal_3/c;
vout3l(1)=0;
end
%Amplitudes
oa2v_a(j,:)=oa2v_A;
oa3v_a(j,:)=oa3v_A;
vout1l_v(j,:)=vout1l;
vout2l_v(j,:)=vout2l;
%%  Calculate the output POSITION 2
%Longitudinal
H22l=[vout2l conj(fliplr(vout2l))];
f1=0:df:fs;
H22l=H22l(1:length(f1));
ht2=(ifft(H22l));
vout2l_vt(j,:)=ht2;
% without convolution
V2wc=FT.*H22l;
v2=ifft(V2wc);
V2wc=V2wc(1:length(f));
V2_v(j,:)=V2wc;
v2_v(j,:)=v2;
%%  Calculate the output POSITION 1
%Longitudinal
H11l=[vout1l conj(fliplr(vout1l))];
f1=0:df:fs;
H11l=H11l(1:length(f1));
ht1=(ifft(H11l));
vout1l_vt(j,:)=ht1;
% without convolution
XO=FT.*H11l;
v1=ifft(XO);
XO=XO(1:length(f));
V1_v(j,:)=XO;
v1_v(j,:)=v1;
%% Calculate the output POSITION 3 (this is only to normalize the sensor 1)
%Longitudinal
H33l=[vout3l conj(fliplr(vout3l))];
f1=0:df:fs;                             % only for num. of values of f1
H33l=H33l(1:length(f1));
ht33=(ifft(H33l));
% without convolution
X33=FT.*H33l;
v33=ifft(X33);
X33=X33(1:length(f));
%% Quantification
px1=sum(sqrt((v1_v(j,:).^2)))/sum(sqrt((v33).^2));
py1=sum(sqrt((v2_v(j,:).^2)))/sum(sqrt((v2_v(1,:)).^2));
px1_s1(j,1)=px1;
py1_s2(j,1)=py1;
px2=sum(((v1_v(j,:).^2)))/sum(((v33).^2));
py2=sum(((v2_v(j,:).^2)))/sum(((v2_v(1,:)).^2));
px2_s1(j,1)=px2;
py2_s2(j,1)=py2;
end
```

```
% CASE SYMMETRIC-LONGITUDINAL WAVE
%% AMPLITUDE OF REFLECTED AND TRANSMITTED WAVE
figure (3)
plot(rld,abs(oa2v_a(1,:)),'b',rld,abs(oa2v_a(10,:)),'r',rld,abs(oa2v_a(20,:)),'g',rld,abs(oa2v_a(30,:)),'k',rld,abs(oa2
v_a(40,:)),'m',rld,abs(oa2v_a(50,:)),'--b',rld,abs(oa2v_a(60,:)),'--r',rld,abs(oa2v_a(70,:)),'--m'...

,rld,abs(oa3v_a(1,:)),'b',rld,abs(oa3v_a(10,:)),'r',rld,abs(oa3v_a(20,:)),'g',rld,abs(oa3v_a(30,:)),'k',rld,abs(oa3v_a(
40,:)),'m',rld,abs(oa3v_a(50,:)),'--b',rld,abs(oa3v_a(60,:)),'--r',rld,abs(oa3v_a(70,:)),'--m')
legend('0%','10%','20%','30%','40%','50%','60%','70%')
set(gca,'fontsize',12,'xlim',[0 1])
title('RATIO OF LENGTH OF DAMAGE TO WAVELENGTH')
xlabel('ratio Ld/\lambda')
ylabel('ratio amplitude ')
%% TRANSFER FUNCTION FREQ DOMAIN PZT 1
figure (4)
loglog(f,abs(vout1l_v(1,:)),'b',f,abs(vout1l_v(10,:)),'r',f,abs(vout1l_v(20,:)),'g',f,abs(vout1l_v(30,:)),'k',f,abs(vout
1l_v(40,:)),'m',f,abs(vout1l_v(50,:)),'--b',f,abs(vout1l_v(60,:)),'--r',f,abs(vout1l_v(70,:)),'--m')
legend('0%','10%','20%','30%','40%','50%','60%','70%')
set(gca,'fontsize',12)
title('TRANSFER FUNCTION FREQ DOMAIN SENSOR 1')
xlabel('Frequency (Hz)')
ylabel('Magnitude')
figure (5)
plot(f,180/pi*unwrap(angle(vout1l_v(1,:))),'b',f,180/pi*unwrap(angle(vout1l_v(10,:))),'r',f,180/pi*unwrap(angle(
vout1l_v(20,:))),'g',f,180/pi*unwrap(angle(vout1l_v(30,:))),'k',f,180/pi*unwrap(angle(vout1l_v(40,:))),'m',f,180/
pi*unwrap(angle(vout1l_v(50,:))),'--b',f,180/pi*unwrap(angle(vout1l_v(60,:))),'--
r',f,180/pi*unwrap(angle(vout1l_v(70,:))),'--m')
legend('0%','10%','20%','30%','40%','50%','60%','70%')
set(gca,'fontsize',12)
title('TRANSFER FUNCTION FREQ DOMAIN SENSOR 1' )
xlabel('Frequency(Hz)');
ylabel('Phase (degrees)');
%% TRANSFER FUNCTION TIME DOMAIN PZT 1
figure (6)
plot(t,vout1l_vt(1,:),'b',t,vout1l_vt(10,:),'r',t,vout1l_vt(20,:),'g',t,vout1l_vt(30,:),'k',t,vout1l_vt(40,:),'m',t,vout1l_v
t(50,:),'--b',t,vout1l_vt(60,:),'--r',t,vout1l_vt(70,:),'--m')
legend('0%','10%','20%','30%','40%','50%','60%','70%')
set(gca,'fontsize',12)
title('TRANSFER FUNCTION TIME DOMAIN SENSOR 1')
xlabel('time ')
ylabel('Magnitude ')
%% TRANSFER FUNCTION FREQ DOMAIN PZT 2
figure (7)
loglog(f,abs(vout2l_v(1,:)),'b',f,abs(vout2l_v(10,:)),'r',f,abs(vout2l_v(20,:)),'g',f,abs(vout2l_v(30,:)),'k',f,abs(vout
2l_v(40,:)),'m',f,abs(vout2l_v(50,:)),'--b',f,abs(vout2l_v(60,:)),'--r',f,abs(vout2l_v(70,:)),'--m')
legend('0%','10%',20','30%','40%','50%','60%','70%')
set(gca,'fontsize',12)
title('TRANSFER FUNCTION FREQ DOMAIN SENSOR 2')
xlabel('Frequency (Hz)')
ylabel('Magnitude (m/Ns)')
figure (8)
plot(f,180/pi*unwrap(angle(vout2l_v(1,:))),'b',f,180/pi*unwrap(angle(vout2l_v(10,:))),'r',f,180/pi*unwrap(angle(
vout2l_v(20,:))),'g',f,180/pi*unwrap(angle(vout2l_v(30,:))),'k',f,180/pi*unwrap(angle(vout2l_v(40,:))),'m',f,180/
pi*unwrap(angle(vout2l_v(50,:))),'--b',f,180/pi*unwrap(angle(vout2l_v(60,:))),'--
r',f,180/pi*unwrap(angle(vout2l_v(70,:))),'--m')
legend('0%','10%','20%','30%','40%','50%','60%','70%')
set(gca,'fontsize',12)
title('TRANSFER FUNCTION FREQ DOMAIN SENSOR 2' )
xlabel('Frequency - log scale(Hz)');
ylabel('Phase (degrees)');
```

```
%% TRANSFER FUNCTION TIME DOMAIN PZT 2
figure (9)
plot(t,vout2l_vt(1,:),'b',t,vout2l_vt(10,:),'r',t,vout2l_vt(20,:),'g',t,vout2l_vt(30,:),'k',t,vout2l_vt(40,:),'m',t,vout2l_v
t(50,:),'--b',t,vout2l_vt(60,:),'--r',t,vout2l_vt(70,:),'--m')
legend('0%','10%','20%','30%','40%','50%','60%','70%')
set(gca,'fontsize',12)
title('TRANSFER FUNCTION TIME DOMAIN SENSOR 2')
xlabel('time ')
ylabel('Magnitude ')
%% OUTPUT IN FREQ DOMAIN PZT 1
figure (10)
loglog(f,abs(V1_v(1,:)),'b',f,abs(V1_v(10,:)),'r',f,abs(V1_v(20,:)),'g',f,abs(V1_v(30,:)),'k',f,abs(V1_v(40,:)),'m',f,a
bs(V1_v(50,:)),'--b',f,abs(V1_v(60,:)),'--r',f,abs(V1_v(70,:)),'--m')
legend('0%','10%','20%','30%','40%','50%','60%','70%')
set(gca,'fontsize',12)
title('OUTPUT FREQ DOMAIN SENSOR 1')
xlabel('Frequency (Hz)')
ylabel('Magnitude (m/Ns)')
figure (11)
semilogx(f,180/pi*unwrap(angle(V1_v(1,:))),'b',f,180/pi*unwrap(angle(V1_v(10,:))),'r',f,180/pi*unwrap(angle(V
1_v(20,:))),'g',f,180/pi*unwrap(angle(V1_v(30,:))),'k',f,180/pi*unwrap(angle(V1_v(40,:))),'m',f,180/pi*unwrap(a
ngle(V1_v(50,:))),'--b',f,180/pi*unwrap(angle(V1_v(60,:))),'--r',f,180/pi*unwrap(angle(V1_v(70,:))),'--m')
legend('0%','10%','20%','30%','40%','50%','60%','70%')
set(gca,'fontsize',12)
title('OUTPUT FREQ DOMAIN SENSOR 1' )
xlabel('Frequency (Hz)');
ylabel('Phase (degrees)');
%% OUTPUT IN TIME DOMAIN PZT 1
figure (12)
plot(t,v1_v(1,:),'-.m',t,v1_v(10,:),':r',t,v1_v(20,:),'g',t,v1_v(30,:),'--g',t,v1_v(40,:),'m',t,v1_v(50,:),'b',t,v1_v(60,:),'-
-r',t,v1_v(70,:),'--m','LineWidth',2)
legend('0%','10%','20%','30%','40%','50%','60%','70%')
set(gca,'fontsize',12,'xlim',[0 tf])
title('Behaviour of damage for wave longitudinal-ratio Ld/\lambda=0.25-sensor1')
xlabel('time (s)')
ylabel('Magnitude')
%% OUTPUT IN FREQ DOMAIN PZT 2
figure (13)
loglog(f,abs(V2_v(1,:)),'b',f,abs(V2_v(10,:)),'r',f,abs(V2_v(20,:)),'g',f,abs(V2_v(30,:)),'k',f,abs(V2_v(40,:)),'m',f,a
bs(V2_v(50,:)),'--b',f,abs(V2_v(60,:)),'--r',f,abs(V2_v(70,:)),'--m')
legend('0%','10%','20%','30%','40%','50%','60%','70%')
set(gca,'fontsize',12)
title('OUTPUT FREQ DOMAIN SENSOR 2')
xlabel('Frequency (Hz)')
ylabel('Magnitude (m/Ns)')
figure (14)
plot(f,180/pi*unwrap(angle(V2_v(1,:))),'b',f,180/pi*unwrap(angle(V2_v(2,:))),'r',f,180/pi*unwrap(angle(V2_v(3,
:))),'g',f,180/pi*unwrap(angle(V2_v(4,:))),'k',f,180/pi*unwrap(angle(V2_v(5,:))),'m',f,180/pi*unwrap(angle(V2_
v(6,:))),'--b',f,180/pi*unwrap(angle(V2_v(7,:))),'--r',f,180/pi*unwrap(angle(V2_v(8,:))),'--m')
legend('0%','10%','20%','30%','40%','50%','60%','70%')
set(gca,'fontsize',12)
title('OUTPUT FREQ DOMAIN SENSOR 2' )
xlabel('Frequency (Hz)');
ylabel('Phase (degrees)');
%% OUTPUT IN TIME DOMAIN PZT 2
figure (15)
plot(t,v2_v(1,:),'-.m',t,v2_v(10,:),':r',t,v2_v(20,:),'g',t,v2_v(30,:),'--g',t,v2_v(40,:),'m',t,v2_v(50,:),'b',t,v2_v(60,:),'-
-r',t,v2_v(70,:),'--m','LineWidth',2)
legend('0%','10%','20%','30%','40%','50%','60%','70%')
set(gca,'fontsize',12,'xlim',[0 tf])
```

```
title('Behaviour of damage for wave longitudinal-ratio Ld/\lambda=0.25-sensor2')
xlabel('time (s)')
ylabel('Magnitude')
%% QUANTIFICATION
dom=1:1:100;
px1_s1(101,1)=1;
py1_s2(101,1)=0;
px2_s1(101,1)=1;
py2_s2(101,1)=0;
figure(16)
plot(dom,px1_s1(2:101,1),'b',dom,py1_s2(2:101,1),'r')
legend('sensor 1','sensor 2','total')
title('DAMAGE INDEX')
ylabel('Damage index 1-2');
xlabel('%Damage');
grid on
figure(17)
plot(dom,px2_s1(2:101,1),'b',dom,py2_s2(2:101,1),'r',dom,px2_s1(2:101,1)+py2_s2(2:101,1),'k')
legend('sensor 1','sensor 2','total')
title('POWER INDEX')
ylabel('Power index 1-2');
xlabel('%Damage');
grid on
```

2. Matlab code for complete system beam-PZT-damage with flexural waves

```
%%
% Simulation using flexural waves of the complete Model with actuator,
% sensor and symmetric damage
% Results
% -Input Voltage in frequency and time domain
% -interaction of the wave with damage
% -IRF and FRF
% -Output Voltage in frequency and time domain
% -Damage Index and Power index
%%
warning off;
clear all;clc;close all;
%% properties of the beam
E=71e9;                 % Young's modulus (N/m2)
rho=2730;               % Density (kg/m3)
b=14e-3;                % width (m)
h=2e-3;                 % thickness (m)
I=b*h^3/12;             % Second moment of area (m3)
A=b*h;                  % Cross-sectional area (m2)
L1=0.395;               % Length before the damage (m)
L2=0.395;               % Length after the damage (m)
EI=E*I;                 % Flexural rigidity
EA=E*A;                 % In-plane stiffness
%% properties of the PZT
%PSI-5A4E PZT from Piezo Systems, INC.
Ea=6.6e10;              % Young's modulus (N/m2)
ha=1.91e-4;             % thickness(m)
ba=14e-3;               % width(m)
d31=-190e-12;           % material strain constant (m/v)
la=0.0068;              % length of actuator
l1=0.0068;              % length of sensor 1
```

```
l2=0.0068;                  % length of sensor 2
c=430e-9;                   % Capacitance of the sensor (F)
%% parameters of signal processing
fs=2000000;                  % (Hz) Sampling Frequency
dt=1/fs;                    % Resolution
tf=8E-3;                    % time
df=1/tf;                    % Resolution
f=0:df:fs/2;                % vector frequency
t=0:dt:tf;                  % vector time
%% parameters of voltage input
freq = 100000;              % frequency of the signal (Hz)
Vin=1;                      % voltage Amplitude
tf1=1e-4;                   % time of the signal (s)
dt1=1/fs;                   % Resolution (s)
t1=0:dt1:tf1;               % vector time of signal (s)
%% voltage input
ftt=zeros(size(t));
ft1=Vin*sin(2*pi*freq*t1);
fh=hann(length(ft1));
fw=fh.*ft1';
ftt(1:length(t1))=fw;
ft=ftt;
FT=fft(ft);



%% Plotting voltage input
% INPUT VOLTAGE TIME DOMAIN
figure (1)
plot(t,ft)
title('INPUT VOLTAGE ON TIME DOMAIN')
xlabel('time (s)')
ylabel('Voltage (V)')

% INPUT VOLTAGE FREQ DOMAIN
figure (2)
semilogx(f,abs(FT(1:length(f))))
title('INPUT VOLTAGE ON FREQ DOMAIN')
xlabel('freq (Hz)')
ylabel('Voltage (V)')
%% Preallocating Arrays

vx1_flex=zeros(1,length(f));
vx1_eva=zeros(1,length(f));
vx1_ex=zeros(1,length(f));
oa22v=zeros(1,length(f));
oa33v=zeros(1,length(f));
lambdab=zeros(1,length(f));
lambda1=zeros(1,length(f));
oa22v_A=zeros(1,length(f));
oa33v_A=zeros(1,length(f));
vout2f=zeros(1,length(f));
vout1f=zeros(1,length(f));
vout3f=zeros(1,length(f));
vout1f_v=zeros(8,length(f));
vout2f_v=zeros(8,length(f));
vout1f_vt=zeros(100,length(t));
vout2f_vt=zeros(100,length(t));
V11_v=zeros(8,length(f));
v11_v=zeros(8,length(t));
```

```
lambdad=zeros(1,length(f));
rbd=zeros(1,length(f));
v22_v=zeros(8,length(t));
V22_v=zeros(100,length(f));
%%
px1_s1=zeros(100,1);
py1_s2=zeros(100,1);
px2_s1=zeros(100,1);
py2_s2=zeros(100,1);

%% different percentage of damages
Dam=0:1:100;
for j=1:101
n=0;
for fq=0:df:fs/2;                    % Frequency
n=n+1;
w=2*pi*fq;
kb=(rho*A/(EI))^.25*w.^.5;           % flexural wavenumber
lambdab(n)=2*pi/kb;
kl=(rho/E)^.5*w;                     % Longitudinal wavelength
lambda1(n)=2*pi/kl;
HB=[0 0 1 0 0 1;
   1 1 0 1 1 0;
   kb 1i*kb 0 -kb -1i*kb 0;
   EI*kb.^2 -EI*kb.^2 0 EI*kb.^2 -EI*kb.^2 0;
   EI*kb.^3 -1i*EI*kb.^3 0 -EI*kb.^3 1i*EI*kb.^3 0;
   0 0 1i*EA*kl 0 0 -1i*EA*kl];
%% state vector-wave matrix of damaged section
% properties of the damaged section of beam
Ld=5/1000;                           % Length of the damaged section
Ed=71e9;                             % Young's modulus
rhod=2730;                           % Density
td=1-Dam(j)/100;
bd=14e-3;hd=2e-3*td;                 % Breadth and depth
Ad=bd*hd;                            % Cross-sectional area
Id=bd*hd^3/12;                       % Second moment of area
EId=Ed*Id;                           % Flexural rigidity
EAd=Ed*Ad;                           % In-plane stiffness
kbd=(rhod*Ad/(Ed*Id))^.25*w.^.5;% flexural wavenumber
kld=(rhod/Ed)^.5*w;                  % Longitudinal wavenumber
lambdad(n)=2*pi/kbd;
rbd(n)=Ld/lambdab(n);
HD=[0 0 1 0 0 1;
   1 1 0 1 1 0;
   kbd 1i*kbd 0 -kbd -1i*kbd 0;
   EId*kbd.^2 -EId*kbd.^2 0 EId*kbd.^2 -EId*kbd.^2 0;
   EId*kbd.^3 -1i*EId*kbd.^3 0 -EId*kbd.^3 1i*EId*kbd.^3 0;
   0 0 1i*EAd*kld 0 0 -1i*EAd*kld];

%% wave transmission ratio defect
TD=[exp(kbd*Ld) 0 0 0 0 0;
   0 exp(1i*(h/hd)^0.5*2*pi*rbd(n)) 0 0 0 0;
   0 0 exp(1i*kld*Ld) 0 0 0;
   0 0 0 exp(-kbd*Ld) 0 0;
   0 0 0 0 exp(-1i*(h/hd)^0.5*2*pi*rbd(n)) 0;
   0 0 0 0 0 exp(-1i*kld*Ld)];
%% wave transmission ratio L1 side (left-right)
TL1=[exp(kb*L1) 0 0 0 0 0;
   0 exp(1i*kb*L1) 0 0 0 0;
   0 0 exp(1i*kl*L1) 0 0 0;
```

```
    0 0 0 exp(-kb*L1) 0 0;
    0 0 0 0 exp(-1i*kb*L1) 0;
    0 0 0 0 0 exp(-1i*kl*L1)];
%% wave transmission ratio L2 side (left-right)
TL2=[exp(kb*L2) 0 0 0 0 0;
    0 exp(1i*kb*L2) 0 0 0 0;
    0 0 exp(1i*kl*L2) 0 0 0;
    0 0 0 exp(-kb*L2) 0 0;
    0 0 0 0 exp(-1i*kb*L2) 0;
    0 0 0 0 0 exp(-1i*kl*L2)];
%% wave transmission ratio L1 side (right-left)
L3=L1+la-l1;
TL3=[exp(kb*-L3) 0 0 0 0 0;
    0 exp(1i*kb*-L3) 0 0 0 0;
    0 0 exp(1i*kl*-L3) 0 0 0;
    0 0 0 exp(-kb*-L3) 0 0;
    0 0 0 0 exp(-1i*kb*-L3) 0;
    0 0 0 0 0 exp(-1i*kl*-L3)];
%% wave_actuator_single - Equation for one side
tt=E*b*h/(Ea*ba*ha);
DD=d31*Vin/ha;
T=ha/h;
M=h^2*E*b*DD*(1+T)/(6+tt+12*T+8*T^2);
% Matrix of Flexural and evanescence wave
Tf=[-1 -exp(kb*la);
     1 exp(1i*kb*la)];
% Flexural Amplitudes generated by the initial wave propagation of PZT
ab0=(4*E*I*kb^2)^-1*Tf*[-M M]';
vx1_flex(n)= ab0(2)*exp(-1i*kb*(la));
vx1_eva(n)=ab0(1)*exp(-kb*(la));
%% Analyzing before the sensor 2 for normalization (quantification)
L=L1+L2;                                    % Position before the sensor 2
vx1_ex=vx1_flex(n)*exp(-1i*kb*(L));
%% Calculate matrices relating the incoming and outgoing waves
ai=[0;0;0;0;vx1_flex(n);0];                 % Wave Amplitude vector initial from actuator 1
a1=TL1*ai;
HH = HD*TD*(HD\HB);
B=[HB(:,1:3) HH(:,4:6)];
C=[HH(:,1:3) HB(:,4:6)];
oa1=C\B*a1;
% position 2
oa2=TL2*oa1;
oa2_6_right=oa2(6);
oa2_5_right=oa2(5);
oa2_4_right=oa2(4);
%flexural
oa22vA=oa2_5_right;
oa22v_A(n)=oa22vA./vx1_flex(n);
oa22v(1)=1;
% position 1
oa3=TL3*oa1;
oa3_3_left=oa3(3);
oa3_2_left=oa3(2);
oa3_1_left=oa3(1);
%flexural
oa33vA=oa3_2_left;
oa33v_A(n)=oa33vA./vx1_flex(n);
oa33v_A(1)=0;
%% Calculate the output voltage in the sensor-2
% flexural difference in the sensor 2
```

```
dif_f2= 1i*kb*oa2(5)*(1-exp(-1i*kb*l2))+kb*oa2(4)*(1-exp(-kb*l2));
% Charge generated by flexural wave
q_flex_2=d31*Ea*ba*(h/2)*dif_f2;
% Voltage total generated in the sensor 2 for all frequencies
vout2f(n)=q_flex_2/c;
% Initial value to avoid Nan
vout2f(1)=0;
%% Calculate the output voltage in the sensor-1
% Evanescent and flexural difference from de defect to sensor 1
dif_f1= (-1)*1i*kb*oa3(2)*(1-exp(1i*kb*(-l1)))...()
    +kb*oa3(1)*(1-exp(kb*(-l1)));
% flexural difference from the actuator to the sensor 1. (Turn off for
% quantification, plots 16-17)
dif_f11=0;%(M/(2*E*I*kb))*(1-exp(-kb*l1)-1i*(1-exp(-1i*kb*l1)));
% Flexural total difference
dif_tot_f=dif_f11+dif_f1;
% Charge generated by flexural waves
q_flex_1=d31*Ea*ba*(h/2)*dif_tot_f;
% Voltage generated in the sensor 1 by flexural waves for all freq.
vout1f(n)=q_flex_1/c;
% Initial value to avoid Nan
vout1f(1)=0;
%% Calculate the output voltage in sensor-3 for quantification sensor 1(this is only to normalize the sensor 1)
% Evanescent and flexural difference from the actuator to the sensor 1
dif_f3= 1i*kb*vx1_ex*(1-exp(-1i*kb*l2));
qtotal_3=d31*Ea*ba*(h/2)*dif_f3;
vout3f(n)=qtotal_3/c;
vout3f(1)=0;
end
%% Amplitudes
oa22v(j,:)=oa22v_A;
oa33v(j,:)=oa33v_A;
vout1f_v(j,:)=vout1f;
vout2f_v(j,:)=vout2f;
%%  Calculate the output POSITION 2
%Flexural
H22f=[vout2f conj(fliplr(vout2f))];
f1=0:df:fs;                          % only for num. of values of f1
H22f=H22f(1:length(f1));
ht22=(ifft(H22f));
vout2f_vt(j,:)=ht22;
% without convolution
V22wc=FT.*H22f;
v22=ifft(V22wc);
V22wc=V22wc(1:length(f));
%FRF
V22_v(j,:)=V22wc;
%IRF
v22_v(j,:)=v22;
%%  Calculate the output POSITION 1
%Flexural
H11f=[vout1f conj(fliplr(vout1f))];
f1=0:df:fs;                          % only for num. of values of f1
H11f=H11f(1:length(f1));
ht11=(ifft(H11f));
vout1f_vt(j,:)=ht11;
% without convolution
XOO=FT.*H11f;
v11=ifft(XOO);
XOO=XOO(1:length(f));
```

```
%FRF
V11_v(j,:)=XOO;
%IRF
v11_v(j,:)=v11;
%% Calculate the output POSITION 3 (this is only to normalize sensor 1)
%Flexural
H33f=[vout3f conj(fliplr(vout3f))];
f1=0:df:fs;                         % only for num. of values of f1
H33f=H33f(1:length(f1));
ht33=(ifft(H33f));
% without convolution
X33=FT.*H33f;
v33=ifft(X33); %inverse because is in antiphase
X33=X33(1:length(f));
%% Quantification
px1=sum(sqrt((v11_v(j,:).^2)))/sum(sqrt((v33).^2));
py1=sum(sqrt((v22_v(j,:).^2)))/sum(sqrt((v22_v(1,:)).^2));
px1_s1(j,1)=px1;
py1_s2(j,1)=py1;
px2=sum(((v11_v(j,:).^2)))/sum(((v33).^2));
py2=sum(((v22_v(j,:).^2)))/sum(((v22_v(1,:)).^2));
px2_s1(j,1)=px2;
py2_s2(j,1)=py2;
end
% CASE SYMMETRIC-FLEXURAL WAVE
%% AMPLITUDE OF REFLECTED AND TRANSMITTED WAVE
figure (3)
plot(rbd,abs(oa22v(1,:)),'b',rbd,abs(oa22v(10,:)),'r',rbd,abs(oa22v(20,:)),'g',rbd,abs(oa22v(30,:)),'k',rbd,abs(oa22v
(40,:)),'m',rbd,abs(oa22v(50,:)),'--b',rbd,abs(oa22v(60,:)),'--r',rbd,abs(oa22v(70,:)),'--m'...
,rbd,abs(oa33v(1,:)),'b',rbd,abs(oa33v(10,:)),'r',rbd,abs(oa33v(20,:)),'g',rbd,abs(oa33v(30,:)),'k',rbd,abs(oa33v(40,
:)),'m',rbd,abs(oa33v(50,:)),'--b',rbd,abs(oa33v(60,:)),'--r',rbd,abs(oa33v(70,:)),'--m')
legend('0%','10%','20%','30%','40%','50%','60%','70%')
set(gca,'fontsize',12,'xlim',[0 1])
title('RATIO OF LENGTH OF DAMAGE TO WAVELENGTH')
xlabel('ratio Ld/\lambda')
ylabel('ratio amplitude ')
%% TRANSFER FUNCTION FREQ DOMAIN PZT 1
figure (4)
loglog(f,abs(vout1f_v(1,:)),'b',f,abs(vout1f_v(10,:)),'r',f,abs(vout1f_v(20,:)),'g',f,abs(vout1f_v(30,:)),'k',f,abs(vout
1f_v(40,:)),'m',f,abs(vout1f_v(50,:)),'--b',f,abs(vout1f_v(60,:)),'--r',f,abs(vout1f_v(70,:)),'--m')
legend('0%','10%','20%','30%','40%','50%','60%','70%')
set(gca,'fontsize',12)
title('TRANSFER FUNCTION FREQ DOMAIN SENSOR 1')
xlabel('Frequency (Hz)')
ylabel('Magnitude (m/N)')
figure (5)
semilogx(f,180/pi*unwrap(angle(vout1f_v(1,:))),'b',f,180/pi*unwrap(angle(vout1f_v(10,:))),'r',f,180/pi*unwrap(a
ngle(vout1f_v(20,:))),'g',f,180/pi*unwrap(angle(vout1f_v(30,:))),'k',f,180/pi*unwrap(angle(vout1f_v(40,:))),'m',f,
180/pi*unwrap(angle(vout1f_v(50,:))),'--b',f,180/pi*unwrap(angle(vout1f_v(60,:))),'--
r',f,180/pi*unwrap(angle(vout1f_v(70,:))),'--m')
legend('0%','10%','20%','30%','40%','50%','60%','70%')
set(gca,'fontsize',12)
title('TRANSFER FUNCTION FREQ DOMAIN SENSOR 1' )
xlabel('Frequency - log scale(Hz)');
ylabel('Phase (degrees)');
hold on
%% TRANSFER FUNCTION TIME DOMAIN PZT 1
figure (6)
plot(t,vout1f_vt(1,:),'b',t,vout1f_vt(10,:),'r',t,vout1f_vt(20,:),'g',t,vout1f_vt(30,:),'k',t,vout1f_vt(40,:),'m',t,vout1f_
vt(50,:),'--b',t,vout1f_vt(60,:),'--r',t,vout1f_vt(70,:),'--m')
```

```
legend('0%','10%','20%','30%','40%','50%','60%','70%')
set(gca,'fontsize',12)
title('TRANSFER FUNCTION FREQ DOMAIN SENSOR 1')
xlabel('time (s)')
ylabel('Magnitude (m/N)')
%% TRANSFER FUNCTION FREQ DOMAIN PZT 2
figure (7)
loglog(f,abs(vout2f_v(1,:)),'b',f,abs(vout2f_v(10,:)),'r',f,abs(vout2f_v(20,:)),'g',f,abs(vout2f_v(30,:)),'k',f,abs(vout
2f_v(40,:)),'m',f,abs(vout2f_v(50,:)),'--b',f,abs(vout2f_v(60,:)),'--r',f,abs(vout2f_v(70,:)),'--m')
legend('0%','10%','20%','30%','40%','50%','60%','70%')
set(gca,'fontsize',12)
title('TRANSFER FUNCTION FREQ DOMAIN SENSOR 2-flexural')
xlabel('Frequency (Hz)')
ylabel('Magnitude (m/N)')
figure (8)
semilogx(f,180/pi*unwrap(angle(vout2f_v(1,:))),'b',f,180/pi*unwrap(angle(vout2f_v(10,:))),'r',f,180/pi*unwrap(a
ngle(vout2f_v(20,:))),'g',f,180/pi*unwrap(angle(vout2f_v(30,:))),'k',f,180/pi*unwrap(angle(vout2f_v(40,:))),'m',f,
180/pi*unwrap(angle(vout2f_v(50,:))),'--b',f,180/pi*unwrap(angle(vout2f_v(60,:))),'--
r',f,180/pi*unwrap(angle(vout2f_v(70,:))),'--m')
legend('0%','10%','20%','30%','40%','50%','60%','70%')
set(gca,'fontsize',12)
title('TRANSFER FUNCTION FREQ DOMAIN SENSOR 2' )
xlabel('Frequency - log scale(Hz)');
ylabel('Phase (degrees)');
hold on
%% TRANSFER FUNCTION TIME DOMAIN PZT 2
figure (9)
plot(t,vout2f_vt(1,:),'b',t,vout2f_vt(10,:),'r',t,vout2f_vt(20,:),'g',t,vout2f_vt(30,:),'k',t,vout2f_vt(40,:),'m',t,vout2f_
vt(50,:),'--b',t,vout2f_vt(60,:),'--r',t,vout2f_vt(70,:),'--m')
legend('0%','10%','20%','30%','40%','50%','60%','70%')
set(gca,'fontsize',12)
title('TRANSFER FUNCTION FREQ DOMAIN SENSOR 2' )
xlabel('time (s)')
ylabel('Magnitude (m/N)')
%% OUTPUT IN FREQ DOMAIN PZT 1
figure (10)
loglog(f,abs(V11_v(1,:)),'b',f,abs(V11_v(10,:)),'r',f,abs(V11_v(20,:)),'g',f,abs(V11_v(30,:)),'k',f,abs(V11_v(40,:))
,'m',f,abs(V11_v(50,:)),'--b',f,abs(V11_v(60,:)),'--r',f,abs(V11_v(70,:)),'--m')
legend('0%','10%','20%','30%','40%','50%','60%','70%')
set(gca,'fontsize',12)
title('OUTPUT IN FREQ DOMAIN SENSOR 1')
xlabel('Frequency (Hz)')
ylabel('Vout/Vin')
figure (11)
semilogx(f,180/pi*unwrap(angle(V11_v(1,:))),'b',f,180/pi*unwrap(angle(V11_v(10,:))),'r',f,180/pi*unwrap(angle
(V11_v(20,:))),'g',f,180/pi*unwrap(angle(V11_v(30,:))),'k',f,180/pi*unwrap(angle(V11_v(40,:))),'m',f,180/pi*un
wrap(angle(V11_v(50,:))),'--b',f,180/pi*unwrap(angle(V11_v(60,:))),'--r',f,180/pi*unwrap(angle(V11_v(70,:))),'-
-m')
legend('0%','10%','20%','30%','40%','50%','60%','70%')
set(gca,'fontsize',12)
title('OUTPUT IN FREQ DOMAIN SENSOR 1' )
xlabel('Frequency - log scale(Hz)');
ylabel('Phase (degrees)');
hold on
%% OUTPUT IN TIME DOMAIN PZT 1
figure (12)
plot(t,v11_v(1,:),'-.m',t,v11_v(10,:),':r',t,v11_v(20,:),'g',t,v11_v(30,:),'--
g',t,v11_v(40,:),'m',t,v11_v(50,:),'b',t,v11_v(60,:),'--r',t,v11_v(70,:),'--m','LineWidth',2)
legend('0%','10%','20%','30%','40%','50%','60%','70%')
set(gca,'fontsize',12,'xlim',[0 0.0005])
```

```
title('Behaviour of damage for wave flexural-ratio Ld/\lambda=0.1-sensor1')
xlabel('time (s)')
ylabel('Vout/Vin')
hold on
%% OUTPUT IN FREQ DOMAIN PZT 2
figure (13)
loglog(f,abs(V22_v(1,:)),'b',f,abs(V22_v(10,:)),'r',f,abs(V22_v(20,:)),'g',f,abs(V22_v(30,:)),'k',f,abs(V22_v(40,:))
,'m',f,abs(V22_v(50,:)),'--b',f,abs(V22_v(60,:)),'--r',f,abs(V22_v(70,:)),'--m')
legend('0%','10%','20%','30%','40%','50%','60%','70%')
set(gca,'fontsize',12)
title('OUTPUT IN FREQ DOMAIN SENSOR 2')
xlabel('Frequency (Hz)')
ylabel('Vout/Vin')
figure (14)
semilogx(f,180/pi*unwrap(angle(V22_v(1,:))),'b',f,180/pi*unwrap(angle(V22_v(10,:))),'r',f,180/pi*unwrap(angle
(V22_v(20,:))),'g',f,180/pi*unwrap(angle(V22_v(30,:))),'k',f,180/pi*unwrap(angle(V22_v(40,:))),'m',f,180/pi*un
wrap(angle(V22_v(50,:))),'--b',f,180/pi*unwrap(angle(V22_v(60,:))),'--r',f,180/pi*unwrap(angle(V22_v(70,:))),'-
-m')
legend('0%','10%','20%','30%','40%','50%','60%','70%')
set(gca,'fontsize',12)
title('OUTPUT IN FREQ DOMAIN SENSOR 2' )
xlabel('Frequency - log scale(Hz)');
ylabel('Phase (degrees)');
hold on
%% OUTPUT IN TIME DOMAIN PZT 2
figure (15)
plot(t,v22_v(1,:),'-.m',t,v22_v(10,:),':r',t,v22_v(20,:),'g',t,v22_v(30,:),'--
g',t,v22_v(40,:),'m',t,v22_v(50,:),'b',t,v22_v(60,:),'--r',t,v22_v(70,:),'--m','LineWidth',2)
legend('0%','10%','20%','30%','40%','50%','60%','70%')
set(gca,'fontsize',12,'xlim',[0 5E-4])
title('Behaviour of damage for wave flexural-ratio Ld/\lambda=0.1-sensor2')
xlabel('time (s)')
ylabel('Vout/Vin')
%% QUANTIFICATION
dom=1:1:100;
px1_s1(101,1)=1;
py1_s2(101,1)=0;
px2_s1(101,1)=1;
py2_s2(101,1)=0;
figure(16)
plot(dom,px1_s1(2:101,1),'b',dom,py1_s2(2:101,1),'r')
title('DAMAGE INDEX')
ylabel('Amplitude ratio 1-2');
xlabel('%Damage');
grid on
hold on
figure(17)
plot(dom,px2_s1(2:101,1),'b',dom,py2_s2(2:101,1),'r',dom,px2_s1(2:101,1)+py2_s2(2:101,1),'k')
legend('sensor 1','sensor 2','total')
title('POWER INDEX')
ylabel('Ratio of power amplitude 1-2');
xlabel('%Damage');
grid on
```